



# **SIMULATION AND DESIGN TRANSMITTER FOR SEABED LOGGING (SBL)**

By

**NUR INTAN MARLYNY BINTI ABD MAJID**

## **FINAL PROJECT REPORT**

**Submitted to the Electrical & Electronics Engineering Programme  
in Partial Fulfillment of the Requirements  
for the Degree  
Bachelor of Engineering (Hons)  
(Electrical & Electronics Engineering)**

**Universiti Teknologi Petronas  
Bandar Seri Iskandar  
31750 Tronoh  
Perak Darul Ridzuan**

**© Copyright 2010**

**by**

**Nur Intan Marlyny Binti Abd Majid, 2010**

# **CERTIFICATION OF APPROVAL**


## **SIMULATION AND DESIGN TRANSMITTER FOR SEABED LOGGING (SBL)**

By

Nur Intan Marlynny Binti Abd Majid

A project dissertation submitted to the  
Electrical & Electronics Engineering Programme  
Universiti Teknologi PETRONAS  
in partial fulfillment of the requirement for the  
Bachelor of Engineering (Hons)  
(Electrical & Electronics Engineering)

Approved by,

  
DR NOORHANA YAHYA  
Associate Professor  
Fundamental & Applied Sciences Department  
Universiti Teknologi PETRONAS, PERAK

Associate Professor Dr. Noorhana binti Yahya

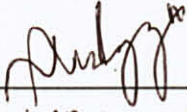
Project Supervisor

UNIVERSITI TEKNOLOGI PETRONAS  
TRONOH, PERAK

JUNE 2010

## CERTIFICATION OF ORIGINALITY

This is to certify that I am responsible for the work submitted in this project, that the original work is my own except as specified in the references and acknowledgements, and that the original work contained herein have not been undertaken or done by unspecified sources or persons.



---

NUR INTAN MARLYNY BT. ABD. MAJID



## ABSTRACT

Seabed logging (SBL) is an application of marine controlled source electromagnetic (CSEM) method which is used to detect the location of oil reservoir. A recently developed transmitter is using Horizontal Electric Dipole (HED) transmitter based on electromagnetic (EM) surveying technique. The technique has proven particularly useful for detecting thin and highly resistive layers of hydrocarbon reservoirs. However, to detect the hydrocarbon reservoirs at very deep seawater still remains a challenge. This project has come out with a new idea of constructing twin curve antenna together with feeders which made from nickel zinc ferrites to enhance the induced magnetic field. Aluminium is the best fit to this project design since it has higher resistance corrosion, light, cheaper than copper and also easy to fabricate. From the CST simulation, the shape of half ring antenna gives greatest improvement on the amplification of EM wave as compared to the ring shape. Later on, the investigation of the thickness and the curvature of the antenna were observed. Three different diameters which is 0.38mm, 1.00mm and 10.00mm were tested and the results showed that the aluminium rod at a diameter of 10.00mm gives highest percentage of 12.79% improvement. The half ring shape gives better result output with a slight increment of 16.80% as compared to the parabolic curvature. The combination of magnetic feeders and the half ring antenna enhanced the output of EM wave with 4 number of toroid gives the maximum amplification signal of 7001%. Other method to amplify the input current signal is by using bridge amplifier. Further improvement to the current design was done by combining two half ring antennas with feeders and as mentioned earlier, it is called as twin curve antenna. This antenna has been tested in a scaled tank filled with salt water and the propagation of EM wave is improved at 388.53% comparing to the earlier design.

## ACKNOWLEDGEMENTS

In the name of God, the Most Gracious, the Most Merciful. Thanks to God for His blessings until this project has come to the end, I managed to complete successfully this Final Year Project. In the first place, I would like to express my deepest appreciation to my supervisor, Associate Professor Dr. Noorhana binti Yahya for her continuous guidance, advice, crucial contribution which made her a backbone to this project until it is completed and enabled me to develop understanding of the project. Without her supervision, this project would be meaningless and it is a pleasure to thank those who made this thesis possible including my team members and postgraduate students under her supervision as well. Without them, there are so many things I could not have gotten such very informative knowledge. It is a pleasure working together in the beam line and we did exchange our knowledge especially during a meeting twice per week and this environment helps me a lot in continuing my research project. Special thanks to the technicians of the Departments of Electrical and Electronics Engineering and Mechanical Engineering of Universiti Teknologi PETRONAS who guided me throughout conducting the experimental works. Not forgotten to my beloved families who'd always been there to keep on supporting me and also to all my fellow friends. Lastly, I offer my regards and blessings to all of those who supported me in any respect during the completion of the project.



# TABLE OF CONTENTS

LIST OF FIGURES.....	ix
LIST OF TABLES .....	xi
LIST OF ABBREVIATIONS .....	xii
CHAPTER 1.....	1
1.1 Background of Study .....	1
1.2 Problem Statement.....	3
1.2.1 Problem Identification.....	3
1.3 Objective and Scope of Study.....	4
CHAPTER 2.....	5
2.1 Literature review.....	5
2.1.1 Seabed logging.....	5
2.1.2 Magnetic feeders.....	6
2.1.3 Square wave current waveform.....	7
2.2 Theory.....	7
2.2.1 Electromagnetic (EM) waves.....	7
2.2.2 Biot Savart Law .....	8
2.2.3 Ampere's Law.....	8
2.2.4 Electrical Properties of Material .....	9
2.2.5 Interference of waves.....	9
2.2.6 Skin Depth.....	10
CHAPTER 3.....	11
3.1 Project Flow Chart.....	11
3.2 Technical design .....	13
3.2.1 Computer Simulation Technology (CST) Software.....	13
3.2.2 Tools and equipments of the experiment.....	13
CHAPTER 4.....	15
4.1 CST Simulation.....	15
4.1.1 Simulation 1 .....	15
4.1.2 Simulation 2 .....	18
4.1.3 Simulation 3 .....	20
4.1.4 Simulation 4 .....	21

4.2 Preliminary Experiments .....	24
4.2.1 Experiment 1: Curvature of the EM transmitter .....	24
4.2.2 Experiment 2: Effect of Diameter/Cross Section of EM transmitter to the B-field.....	26
4.2.3 Experiment 3: Effect of magnetic feeders to the strength of magnetic field .....	28
4.2.4 Experiment 4: Design and Development of Power Bridge Amplifier .....	32
4.2.5 Experiment 5: Effect of Different Position Detector .....	35
4.2.6 Experiment 6: Effect of solenoid to the output magnetic field .....	41
4.2.7 Experiment 7: Prototype design testing in scaled tank filled with salt water.....	44
CHAPTER 5.....	47
5.1 Conclusion .....	47
5.2 Recommendations.....	48
REFERENCES.....	49
APPENDICES.....	52
APPENDIX A.....	53
APPENDIX B .....	60



## LIST OF FIGURES

Figure 1:	Location of HED transmitter and the receivers based on SBL method ..	2
Figure 2:	Propagation of electromagnetic wave .....	7
Figure 3:	An electric current produces a magnetic field.....	8
Figure 4:	Two point source interference pattern.....	10
Figure 5:	Flow chart of the project .....	11
Figure 6:	Instek GFG-8250A Function Generator 5MH.....	14
Figure 7:	Decaport Data Acquisition System.....	14
Figure 8:	Flux gate magnetic field sensor .....	14
Figure 9:	Simulation result of copper rod.....	16
Figure 10:	Simulation result of aluminium rod.....	16
Figure 11:	Graph of comparison between copper and aluminium rod.....	17
Figure 12:	Simulation result of electric field.....	18
Figure 13:	Simulation result of electric flux density.....	18
Figure 14:	Magnetic field over voltage source.....	19
Figure 15:	Graph of electric field vs length of aluminium.....	21
Figure 16:	E-field and B-field for three different configurations.....	22
Figure 17:	Results for three different configurations for simulation 4.....	23
Figure 18:	Two different curvatures of the antennas.....	24
Figure 19:	Bar chart for two types of rod with maximum magnetic field.....	25
Figure 20:	Bar chart for three types of different diameter.....	27
Figure 21:	Illustration for different cross section of aluminium rod and wires.....	27
Figure 22:	Half ring shape of aluminium rod as the transmitter.....	28
Figure 23:	Setup diagram of the experiment 3.....	28
Figure 24:	Nickel Zinc Ferrites with copper windings as magnetic feeder.....	29

Figure 25:	AVO of magnetic field over a distance .....	30
Figure 26:	Amplitude versus offset for observation of curve transmitter.....	31
Figure 27:	Circuit design of 20W power bridge amplifier.....	32
Figure 28:	Setup of the experiment 4.....	32
Figure 29:	Circuit diagram of 20W power bridge amplifier.....	33
Figure 30:	A comparison between two different configurations of the antenna...	34
Figure 31:	Detector at 'r' distance.....	35
Figure 32:	Detector at '2r' distance.....	35
Figure 33:	Result of configuration 1 for experiment 5.....	37
Figure 34:	Pattern of magnetic field of curve antenna.....	37
Figure 35:	Result of configuration 2 for experiment 5.....	40
Figure 36:	Magnetic field lines of a loosely wound solenoid.....	41
Figure 37:	A curve antenna with windings.....	41
Figure 38:	Twin curve antenna with two set of windings.....	41
Figure 39:	Setup of the experiment 6.....	42
Figure 40:	Twin curve aluminium rod.....	42
Figure 41:	Front view of twin curve antenna.....	42
Figure 42:	Bar chart for two different configurations.....	43
Figure 43:	Resistivity meter.....	44
Figure 44:	Water tank filled with saltwater.....	44
Figure 45:	Setup of the experiment 7.....	45
Figure 46:	Result of the experiment 7.....	45
Figure 47:	Middle position of magnetic feeders based on the existing design....	48
Figure 48:	Center position of magnetic feeders.....	48
Figure 49:	End position of magnetic feeders.....	48

## LIST OF TABLES

Table 1:	Conductivity of some common conductor at 20 <sup>0</sup> C.....	9
Table 2:	Setup for the antenna in CST EM studio.....	15
Table 3:	Results for simulation 1.....	17
Table 4:	Setup of the antenna.....	18
Table 5:	Result for simulation 2.....	19
Table 6:	Setup for the 3 <sup>rd</sup> simulation.....	20
Table 7:	Result for simulation 3.....	20
Table 8:	Setup for the 4 <sup>th</sup> simulation.....	22
Table 9:	Simulation result for the 4 <sup>th</sup> simulation.....	23
Table 10:	Setup of the experiment 1.....	24
Table 11:	Result for experiment 1.....	25
Table 12:	Different thickness of aluminium.....	26
Table 13:	Result for experiment 2.....	26
Table 14:	Setup of the experiment 3.....	28
Table 15:	Requirements of magnetic feeders.....	29
Table 16:	Result for experiment 4.....	34
Table 17:	Result of configuration 1 with an illustration of setup diagram.....	36
Table 18:	Result of configuration 1 with an illustration of setup diagram .....	37
Table 19:	Result for experiment 6.....	43
Table 20:	Summary of the prototype design.....	46



## **LIST OF ABBREVIATIONS**

SBL	Seabed Logging
EM	Electromagnetic
HED	Horizontal Electric Dipole
Hz	Hertz
CSEM	Marine Controlled Source Electromagnetic



# CHAPTER 1

## INTRODUCTION

### 1.1 Background of Study

Seabed logging (SBL) is an application of the marine controlled source electromagnetic (CSEM) method which is used to detect the location of the oil reservoir. This method has been used for the past three decades and the application as a direct hydrocarbon indicator was introduced for about five years ago [1]. The SBL method is based on the idea of transmitting the signal from the transmitter which located above the subsurface under the seawater and the wave will be guided along the thin resistive layers within conductive sediments. The implication is that the EM data have the potential to increase the detection rates by 50% or even more [2]. This method includes broadcasting an EM signal from a horizontal electric dipole (HED) transmitter and the response of it will be detected by the receivers which are located on the seafloor.

Referring to Figure 1, the EM signal which comes from HED transmitter is propagated along the seawater and it will penetrate through the subsurface until it reaches the hydrocarbon reservoir. The electromagnetic signals can propagate from the conductive regions to the resistive regions. Under this condition, the signal which comes from conductive region, the seawater; will be guided horizontally along the reservoir and reflected back to the seafloor. In a relatively thin and high resistivity subsurface layer ( $\sim 20\text{-}1000\ \Omega\text{m}$ ), EM energy propagates at a higher velocity but with less attenuation as a guided wave and it is transmitted back to the receivers at the seafloor [3]. As compared to the resistivity of the seawater which is only  $0.25\ \Omega\text{m}$  its makes contrast for about 400 scaled.

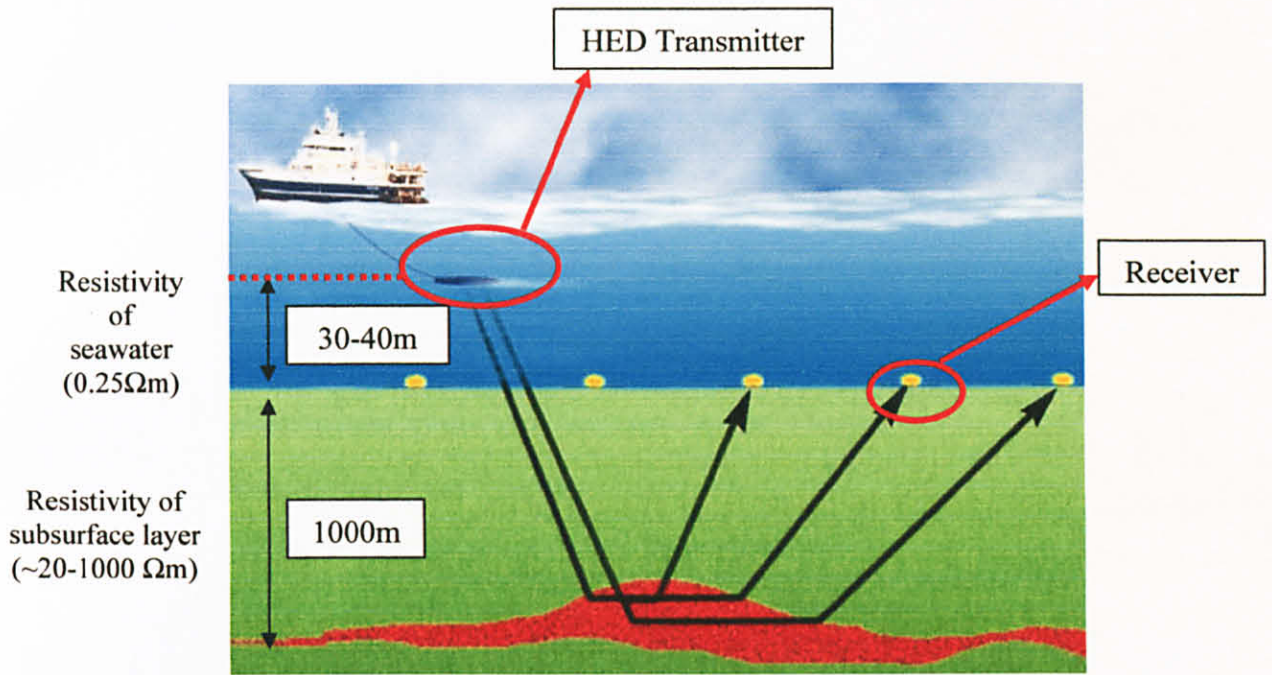


Figure 1: Location of HED transmitter and the receivers based on SBL method [4]

The nearest detector will detect the reflected signal and gives response to the data logger. The recorded data will be sent to the surface for further data analysis. This is how the current technology is used to detect hydrocarbon reservoir. Drilling of well which incurred cost and provide no guarantee can be avoided.

## **1.2 Problem Statement**

### **1.2.1. Problem Identification**

Seismic technology is currently developed to identify the existence, location and extent of reservoirs in subterranean rock strata [5]. However, this technology is unable to distinguish between the different possible compositions of pore fluids within them and this has made the success rate of the exploration wells only about 10-30% [5,6]. Another technology recently developed is using HED transmitter based on electromagnetic (EM) surveying technique and this method is able to distinguish between water and hydrocarbon due to their high different in resistivity value. However, to detect the hydrocarbon at very deep seawater still remains a challenge and yet to find any solution. A transmitter that can boost up the EM signal up to 289% at 100m was previously designed and developed by using this technique [7]. Another great improvement based on the existing design is vital to this project.



### **1.3 Objective and Scope of Study**

The purpose of this project is to design powerful EM transmitter that can produce higher magnitude of EM wave with magnetic feeders as secondary tools to enhance the induced magnetic field. Upon completing the fabrication of the antenna, simulation of design antenna will be done first to validate output result. Testing and experimental work will be performed to demonstrate the capability of transmission electromagnetic wave.

There are several objectives of this project;

- To develop a new design of EM transmitter by using CST software.
- To validate the data simulation by producing a prototype together with magnetic feeders.
- To increase the input current signal by employing full bridge power amplifier.
- To demonstrate MVO (Magnitude Versus Offset) studies in the scaled tank with salt water.



## **CHAPTER 2**

### **LITERATURE REVIEW AND THEORY**

#### **2.1 Literature review**

##### **2.1.1 Seabed logging**

Seabed logging is an application of marine CSEM which are used to detect and characterize hydrocarbon reservoirs in deep water areas. The basis of the approach is the use of horizontal electric dipole (HED) source which generates ultra low frequency ( $\sim 10^{-1}$ -5Hz) but powerful electromagnetic (EM) signals which being towed approximately 30-40 m above the seabed [3]. The dipole emits a low frequency signal into the surrounding media, and the signal is then be recorded by stationary seafloor receivers having both magnetic and electric dipole antennas [8].

The transmitting energy which comes from very low frequency sources tends to attenuate in seawater along with seafloor sediments saturated with conductive saline water. Therefore, it is not that efficient to transmit the signal at very high range of deep water. The rate of decay in amplitude of the electromagnetic energy is controlled by geometric and by skin depth effect. Because in general the seabed is more resistive than seawater, skin depths in the seabed are longer.

Overview by T. Eidesmo et al. [5] described that the effect of the reservoir on the survey results will depend strongly on the direction of flow of the currents generated by the transmitter or the direction of the electrical fields. When the electromagnetic energy is transmitted, the magnetic field will be polarized transversely to the resistive hydrocarbon layer and this is known as transverse magnetic mode, TM mode.

In the TM mode, the magnetic field enters the resistive hydrocarbon layer under a critical angle and propagates along the layer [5]. Due to lower conductivity sediments of the layer, the electrical field will be attenuated less and be guided along the layer. The EM energy which constantly propagates along the reservoir will be back to the seafloor. This guiding of electric field will give the overall performance of the hydrocarbon structure.

### **2.1.2 Magnetic feeders**

Overview from F.N. Kong and H.Westerdahl in their paper of excitation of long wire antenna state that the magnetic feeder constructed by a toroid coil on a ferrite ring can generate strong magnetic field [9]. The power delivered to the ferrite core generates the magnetic flux inside it. When a metal cylinder of conductor is inserted at the middle of the ferrite core, the energy of the magnetic flux will transfer into the current flowing along the antenna conductor. At high frequency the core loss becomes high, which leads to a low efficiency but wide bandwidth of antenna is produced. At this paper, an experiment was conducted where the efficiency of ferrite core in feeding long wire antennas by using only two ferrite rings is to be observed. From the result, it is proved that the utilization of magnetic feeder can enhance the magnetic field of the dipole antenna.

Another view is that they applied low electromagnetic wave frequencies to detect hydrocarbon layer inside seabed and the typical frequency is 0.1-5Hz. It is shown that higher permeability ferrite material is one of the vital properties in making antennas working at that lower frequency range. One of the advantages of using magnetic feeder is that there is no physical contact between the feeder and the wire in which they can place the feeder at an optimum location to achieve best impedance matching.



### 2.1.3 Square wave current waveform

Square wave is frequently used as the transmitter waveform in marine controlled-source electromagnetic or in seabed logging [10]. This type of waveform is easy to generate and it has the advantage of transferring maximum energy to the subsurface of seawater due to the transmitter current is running at its peak amplitude at all times. For a half period of time switching, the electric dipole transmitter is running at maximum current at one polarity. The frequency domain current amplitudes of the square wave are proportional to the inverse of the frequency. Therefore, the current amplitudes are reduced with increased frequency and at the same time the electromagnetic field is easily to absorb when the frequency is higher.

## 2.2 Theory

### 2.2.1 Electromagnetic (EM) waves

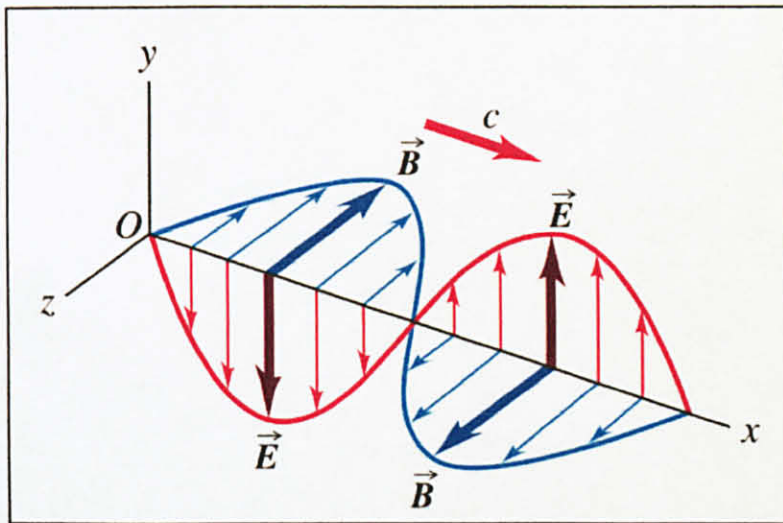


Figure 2 : Propagation of electromagnetic wave [11]

Electromagnetic waves are transverse wave that have some electrical and magnetic properties. It consists of electrical field and magnetic field which are perpendicularly to each other as per illustrated in Figure 2. Maxwell's law of electromagnetism state that a changing electric field will generate a magnetic field, and thus changing magnetic field will induce an electric field [12].

### 2.2.2 Biot Savart Law

The Biot–Savart law is an equation in electromagnetism that describes the magnetic field  $\mathbf{B}$  generated by an electric current [11]. The magnetic field  $\mathbf{B}$  is directly proportional to the current flowing along the material and a distance between the antenna and the receiver also affects the magnitude of the magnetic field. Based on Biot Savart law, the magnetic field  $B$  is given in the following equation:

$$B = \frac{\mu_0 I}{2 \pi R} \quad [11]$$

where  $R$  is the distance between the antenna and the point in space and  $\mu_0$  is the permeability of free space which gives a value of  $4\pi \times 10^{-7}$  A/m. Also, we can observe the direction of the magnetic field which can be determined based on the right hand rule as per shown in Figure 3:

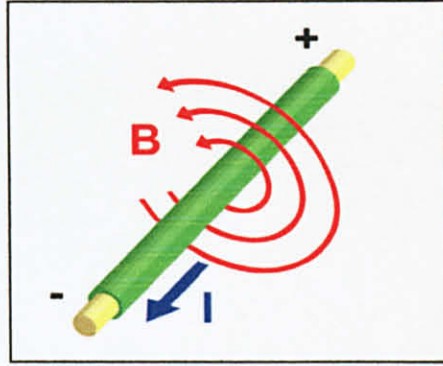


Figure 3: An electric current produces a magnetic field [13]

### 2.2.3 Ampere's Law

Ampere's Law states that for any closed loop path, the sum of the length elements times the magnetic field in the direction of the length element is equal to the permeability times the electric current enclosed in the loop [10]. The current flowing under the material is directly proportional to the integral magnetic field.

$$\oint_C \mathbf{B} \cdot d\boldsymbol{\ell} = \mu_0 I_{\text{enc}} \quad [11]$$

where,  $\oint_C$  is the closed line integral around the closed curve  $C$  and  $I_{\text{enc}}$  is the net free current that penetrates through the surface  $S$ .



## 2.2.4 Electrical Properties of Material

There are three main electromagnetic constitutive parameters of a material medium. They are; electrical permittivity  $\epsilon$ , magnetic permeability  $\mu$ , and conductivity  $\sigma$ . The conductivity of a material is a measure of how easily electrons can travel through the material under the influence of an external electric field [11]. Based on the table shown below, silver shows the highest value of conductivity followed by copper and aluminium. Even though it has higher conductivity, it is still quite expensive as compared to the copper and aluminium. Therefore in our application we will consider only these two materials which are easily available in the lab.

Table 1: Conductivity of some common materials at 20°C [11]

MATERIAL	CONDUCTIVITY, $\sigma$ (S/m)
Silver	$6.2 \times 10^7$
Copper	$5.8 \times 10^7$
Gold	$4.1 \times 10^7$
Aluminium	$3.5 \times 10^7$
Iron	$10^7$
Mercury	$10^6$
Carbon	$3 \times 10^4$

## 2.2.5 Interference of waves

Interference will occur when two or more waves that come from the same sources and same frequency coherently to each other. The waves will be combined together depending on resultant displacement at a point is equal to the vector sum of the displacements of different waves at that point [14]. When the waves are in phase with each other, the constructive interference will occur and the resultant amplitude is twice as large as the amplitude of an individual wave. While destructive interference occurs when waves come together in such a way that they completely cancel each other.

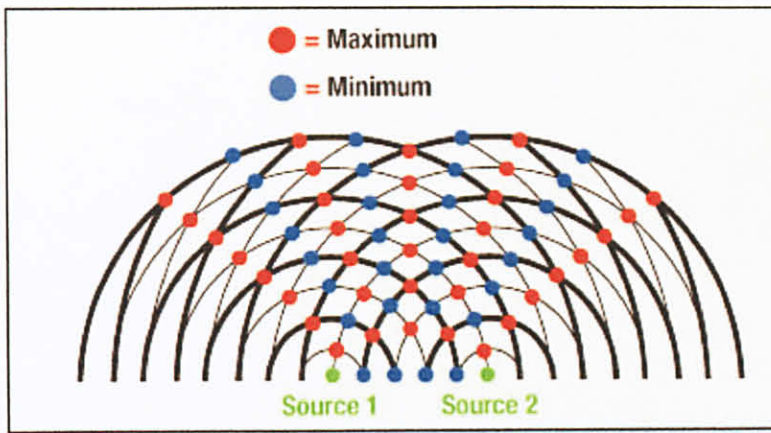


Figure 4: Two point source interference pattern [15]

### 2.2.6 Skin Depth

The skin depth is very important in hydrocarbon exploration. Skin depth can be defined as the depth of electromagnetic wave that can penetrate below the surface of the conductor (seawater) at which the current density decays for about 0.37 factor given by:

$$\delta = \sqrt{\frac{2}{\mu\omega\sigma}} \quad [16]$$

where  $\mu$  is the magnetic permeability of conductor,  $\omega$  is the angular frequency of current and  $\sigma$  is the electrical conductivity of the metal. From the formula shows above, the skin depth varies with the square root of the wavelength. Hence, in order to increase the skin depth, the wavelength should be higher and the frequency used to transmit the EM wave should be lower [17].

## CHAPTER 3

### METHODOLOGY

#### 3.1 Project Flow Chart

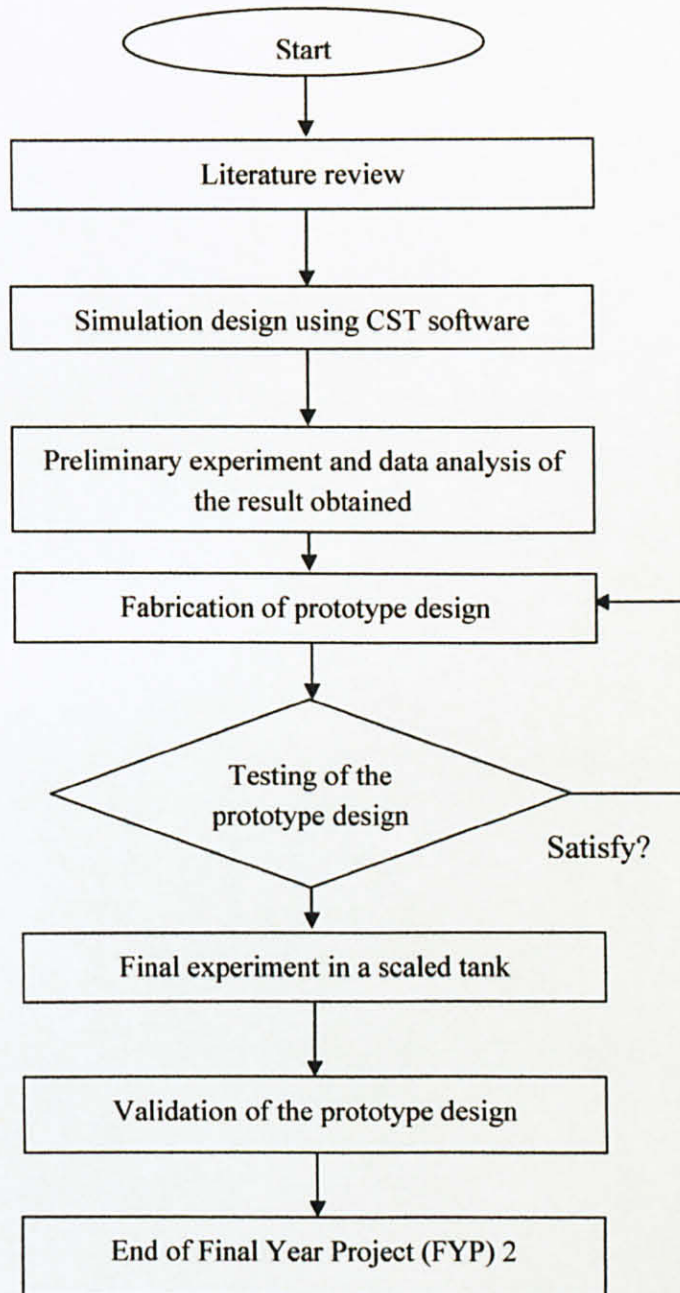


Figure 5: Flow chart of the project



There are several steps involved upon completing this project which can be divided into five main parts.

- Research and literature review
- Simulation design using CST software
- Preliminary experiments in the lab
- Fabrication prototype design
- Testing prototype design in a scaled tank

The first part of this project is devoted to literature survey. The topics include Sea Bed Logging (SBL), electromagnetic concept, magnetic feeder enhancement and some other relevant theories together with the current technology used in hydrocarbon exploration are critically reviewed. This is essential to get an overview of the project before running the simulation. The fundamental of electromagnetic wave is very important in order to apply to this project so that any problem facing later on can be encountered easily.

After completing the research studies, the next step is to simulate the antenna design by using CST software. This is an initial stage to develop the antenna design which includes verification on the material selection and also the shape of the antenna that can affect the simulation results. Details of this design will be explained under the results and discussions.

From the simulation result, the best shape of the antenna design will be chosen to continue with the lab experiment. This lab experiment is aimed to select the best antenna design that gives powerful enhancement of EM wave. By employing the magnetic feeders to the antenna, the resultant output is boosted up several times that gives higher amplification. After that, the fabrication of the antenna will be performed before proceed to the next stage of the project.

The final stage of this project is by testing the antenna's capability in placing them in a large tank surrounding by salt water. This condition is to provide a conductive medium for the EM wave to propagate more effectively as compared in the air.

## **3.2 Technical design**

### **3.2.1 Computer Simulation Technology (CST) Software**

CST EM studio is the most suitable software that can be used to create the first prototype design. It enables full 3-dimension simulation in a wide application range that can be used to simulate various design of the antenna. Various shapes of transmitter design can be created to observe the output results. The results of EM wave can be presented in a form of electrical field, magnetic field, electric flux density and also magnetic field intensity. Therefore, a data analysis can be made in order to select the best design of the antenna.

Various applications in this software can be found which includes actuators, brakes, generators, motors, sensors, switches, and also shielding effect. It provides both orthogonal and tetrahedral meshing in one 3D EM simulator and also three types of solver that can be used in running the simulation which includes electrostatic solver, magnetostatic solver and also full wave solver. The solver which depends on the needs of different sources and the materials must be chosen correctly.

### **3.2.2 Tools and equipments of the experiment**

#### **3.2.2.1 Transmitter**

The purpose of a transmitting antenna is to generate a useful electromagnetic field at a distance [18]. A transmitter can be made from many types of conductor. In this project, the material of the antenna is aluminum since it provides higher propagation of EM wave, light, and can withstand to the corrosion and also easy to fabricate. It is functioning to transmit the electromagnetic wave.

#### **3.2.2.2 Function generator**

The function generator of brand model Instek GFG-8250A is used to generate EM wave and the minimal frequency of 1kHz is selected to ensure that the waveform can be transmitted in a long range. Besides that, at frequencies of 1 kHz, the power loss in the internal resistance of the conductor is negligible and all power is either radiated or transferred to the terminations without loss [18].



The maximum rating of 5MHz is applied if the main concern is to supply higher concentrating EM wave. Without function generator, there is no power supply to the antenna and the EM wave cannot be produced. The output signal can be varied up to the maximum amplitude of 20V peak-to-peak. As per mentioned earlier in the literature review, the square wave transferred the maximum energy to the subsurface of seawater since it is running at the peak amplitude at all times [10].



Figure 6 : Instek GFG-8250A Function Generator 5MHz

### 3.2.2.3 Decaport data acquisition system

The function of the receiver is to detect the received signal and transfer the waveform to the data logger. The same concept is applied to this leading technology system where the magnetic field produced from EM wave can be sensed by fluxgate magnetic field sensor of brand model Mag-03MSS100. This sensor is then connected to the decaport data acquisition system (DAS) Model NI PXI-1042 for the configuration purposes. The fluxgate can detect EM wave in three different directions which are Hx, Hy and Hz.

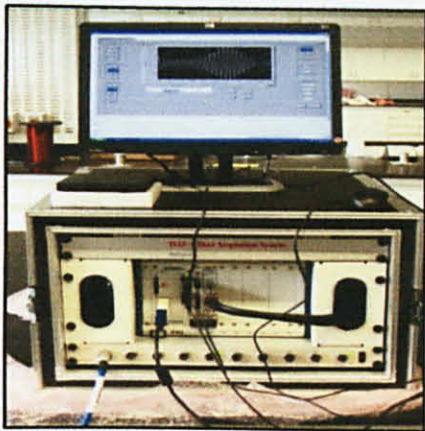


Figure 7: Decaport data acquisition system



Figure 8: Flux gate magnetic field sensor



**CHAPTER 4**  
**RESULTS AND DISCUSSION**

**4.1 CST Simulation**

**4.1.1 Simulation 1**

The first simulation was to compare the strength of EM wave between copper rod and aluminium rod. From the Table 1, copper material gives higher value of conductivity than aluminium. It can be defined that the more conductive of the material, the easiest electrons to flow and they can emits the EM wave easily. This can be proven by running the simulation in both condition of material. Below is the setup parameter of the antenna and the simulation result is shown at Table 3.

Table 2: Setup for the antenna in CST EM studio

SPECIFICATIONS	DETAILS
Frequency	1kHz
Supply voltage	20V
Diameter (dipole)	0.4mm
Length	50mm
Material(s)	Coppber and aluminium
Shape	Rod

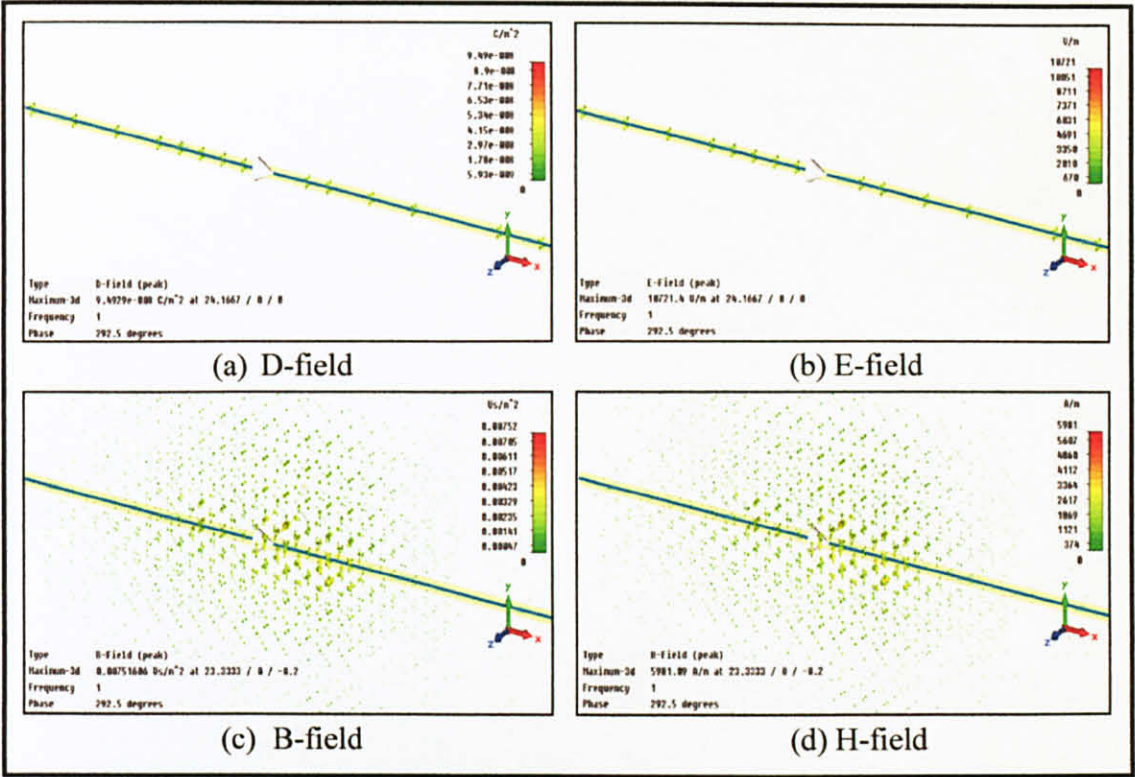


Figure 9: Simulation results of copper rod

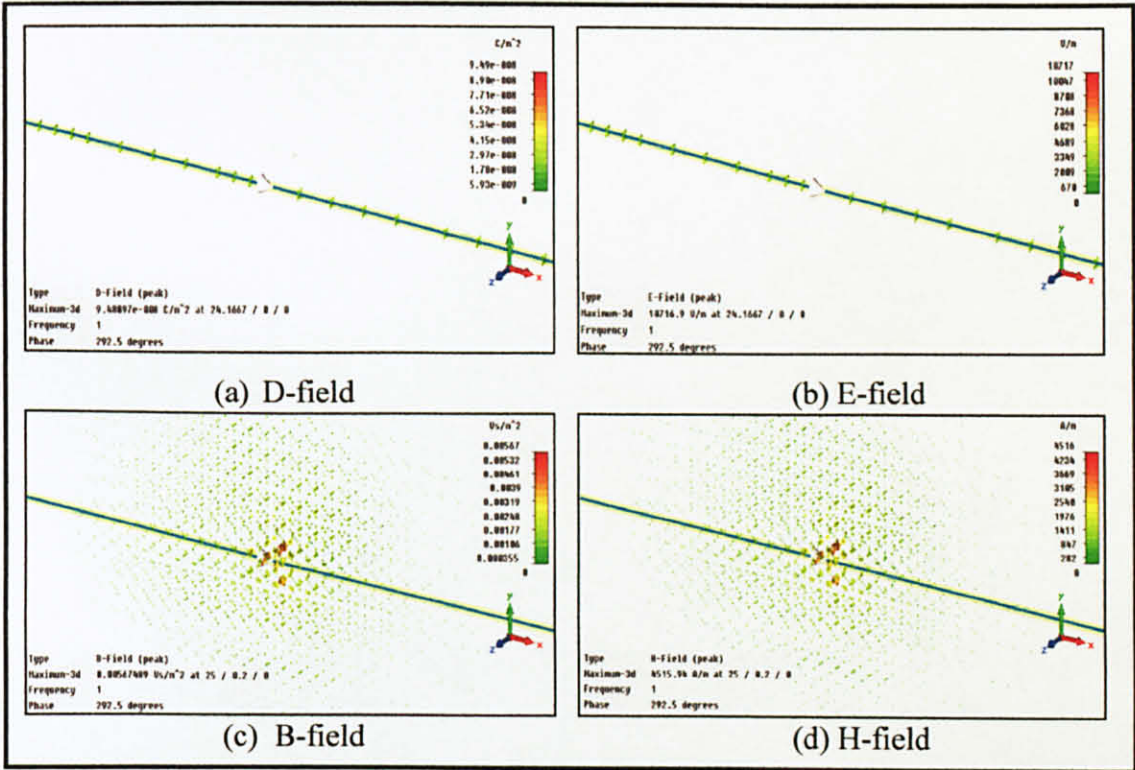


Figure 10: Simulation results of aluminium rod

Table 3: Result for simulation 1

TYPES OF MATERIAL	D-field (C/m <sup>2</sup> )	E-field (V/m)	B-field (Vs/m <sup>2</sup> )	H-field (A/m)
Aluminium	$6.28 \times 10^{-13}$	$7.089 \times 10^{-2}$	$9.74 \times 10^{-7}$	0.7754
Copper	$9.06 \times 10^{-13}$	0.1023	$2.11 \times 10^{-6}$	1.67846

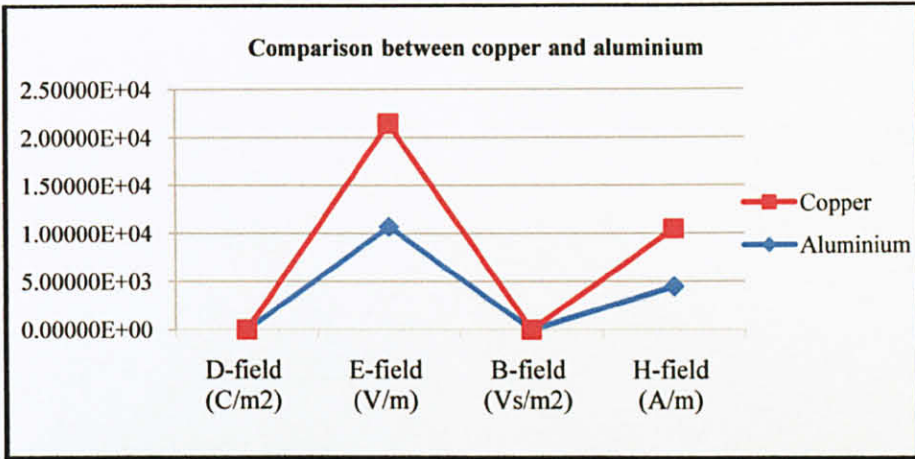


Figure 11: Graph of comparison between copper and aluminium rod

From the result recorded, copper rod gives higher value for D-field, E-field, B-field and H-field. Moreover, by observing the simulation result of Figure 9 (c) and Figure 10 (c), it is clearly seen that the alignment of magnetic field is greater at the copper rod. Electromagnetic wave consists of magnetic field and electric field. The contribution of electric field is higher than magnetic field based on the result obtained where the generated output is amplified at 44.31%. Even though the copper rod can generate electromagnetic wave slightly higher than aluminium, other factors need to be taken into consideration such as the cost, and also the ability to withstand able to the corrosion under the seawater at high pressure and high temperature condition. A copper rod is initially being processed from the continuous casting system yield lower tensile strength and lower hardness [20]. Therefore, it can be concluded that aluminium is the best fit to this project design since it has higher resistance corrosion, light, cheaper than copper and also easy to fabricate.



4.1.2 Simulation 2

For the next approach, we want to observe the effect of the voltage source over the electrical field, magnetic field, electric flux density and also magnetic field intensity. We fixed the length of the antenna at 1m and also the diameter at 0.005m. Below is the setup for the antenna used in our simulation and the results of the experiment:

Table 4: Setup of the antenna

SPECIFICATION	DETAILS
Types of material	Aluminium
Shape	Cylinder
Diameter (meter)	0.01 m
Length (meter)	1m
Electrical conductivity	$3.50 \times 10^7$ S/m
Frequency	1kHz
Boundary condition	Magnetostatic

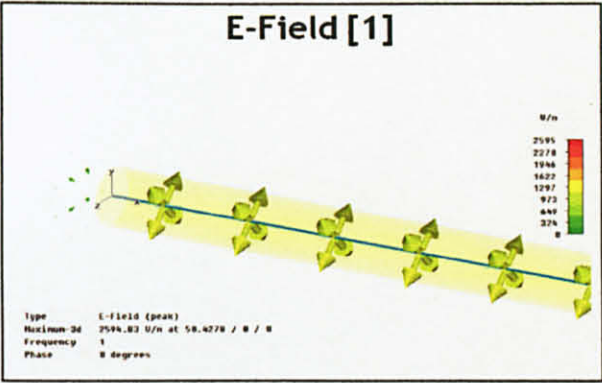


Figure 12: Simulation result of electric field

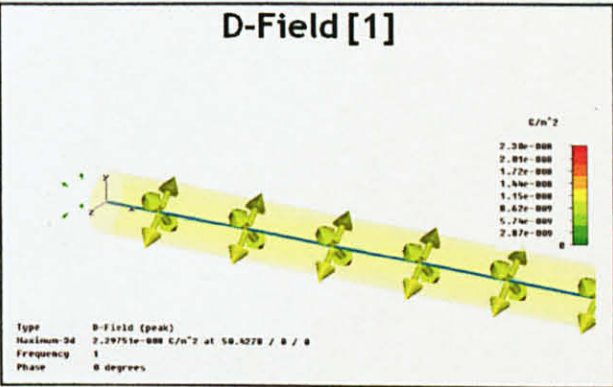


Figure 13: Simulation result of electric flux density

Table 5: Result for Simulation 2

Voltage Source	5V	10V	15V	20V
E-Field (V/m)	1297.42	2594.83	3892.25	5189.66
B-Field (T)	$1.77628 \times 10^{-3}$	$3.55256 \times 10^{-3}$	$5.32885 \times 10^{-3}$	$7.10513 \times 10^{-3}$
D-Field (C/m <sup>2</sup> )	$1.14876 \times 10^{-8}$	$2.2975 \times 10^{-8}$	$3.44627 \times 10^{-8}$	$4.59503 \times 10^{-8}$
H-Field (A/m)	1413.52	2827.04	4240.56	5654.08

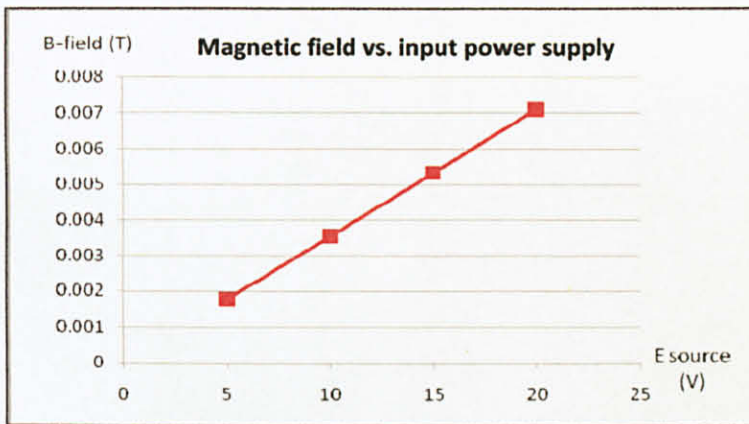


Figure 14 : Magnetic field over voltage source

Based on the table 5 and from the graph shown above, we can see a relationship between the voltage source supplied to the conductor rod is directly proportional to the E-field, B-field, D-field and H-field. The magnetic field is amplified at 300.00% from 5V to 20V. Thus, a conclusion that can be made is that the higher value of voltage source supplied to the antenna, yields higher output of transmission of electromagnetic waves.

4.1.3 Simulation 3

The relationship between the length of the antenna over the electric field and magnetic field was investigated in this simulation. The length of the antenna is one the main factor that affects the performance of the transmitting signal from the transmitter to the receiver. The current source supplied to the antenna is fixed to the 20A and other specifications are shown at Table 6:

Table 6: Setup for the 3<sup>rd</sup> simulation

SPECIFICATION	DETAILS
Types of material	Aluminium rod
Frequency	1kHz
Diameter	0.9mm
Length of variation (cm)	50, 70,90,110,130,150,170,190,210
Boundary condition	Magnetostatic

Table 7: Result for simulation 3

Length (cm)	Electric field (V/m)	Magnetic field (T)
50	$1.545 \times 10^{-3}$	$2.05 \times 10^{-15}$
70	$2.072 \times 10^{-3}$	$3.17 \times 10^{-15}$
90	$2.585 \times 10^{-3}$	$4.73 \times 10^{-15}$
110	$3.07 \times 10^{-3}$	$6.04 \times 10^{-15}$
130	$3.545 \times 10^{-3}$	$8.02 \times 10^{-15}$
150	$3.996 \times 10^{-3}$	$9.71 \times 10^{-15}$
170	$4.438 \times 10^{-3}$	$1.20 \times 10^{-14}$
190	$4.863 \times 10^{-3}$	$1.45 \times 10^{-14}$
210	$5.266 \times 10^{-3}$	$1.65 \times 10^{-14}$



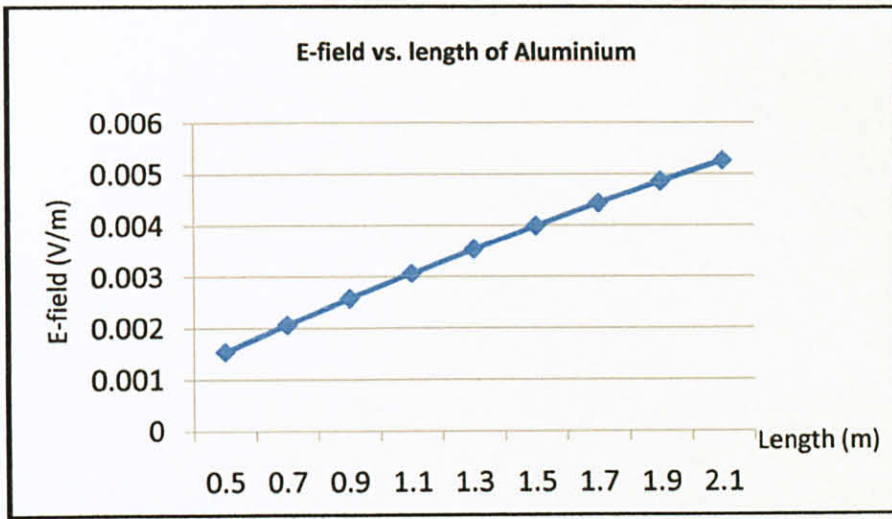


Figure 15: Graph of electric field vs length of aluminium

From the result, as we increased the length of the aluminium rod, the value of the electric field and also the magnetic field is increased. We can use equation [11] to calculate and validate Table 7 results. The magnetic field in space is proportional to the electric current along with the sum of the length elements. We can prove that the signal is strengthen when we increase the length of the antenna by 240.84%.

#### 4.1.4 Simulation 4

From the simulation 3, as we increased the length of the antenna, higher electric field and magnetic field is produced which yield greater result output. Thus, for this simulation, 200cm is to be chosen for the length of the antenna. The variation of configuration will be investigated and the antenna is designed to the three different shape; straight, ring, and half ring.

Table 8: Setup for the 4<sup>th</sup> simulation

SPECIFICATIONS	DETAILS
Material	Aluminium
Diameter (Rod)	0.9mm
Length	200cm
Outer Diameter (Ring)	64cm
Inner Diameter (Ring)	63.1cm
Outer Diameter (Half ring)	127cm
Inner Diameter (Half ring)	126.1cm

Below is the simulation result for three different configurations:

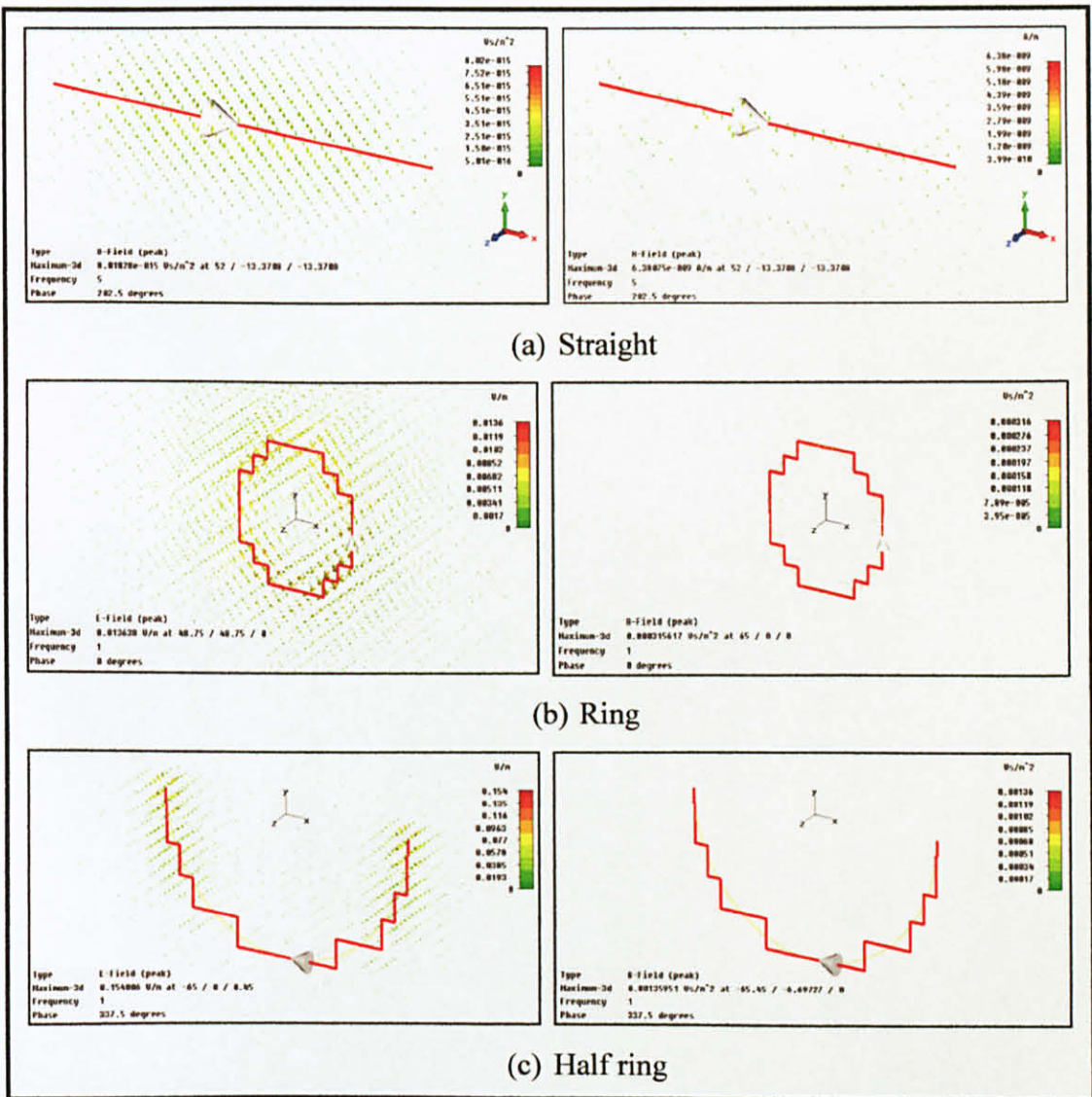


Figure 16: E-field and B-field for three different configurations

Table 9: Simulation result for the 4<sup>th</sup> simulation

SHAPE OF TRANSMITTER	E-field (V/m)	B-field (Vs/m <sup>2</sup> )
Straight	$4.86283 \times 10^{-3}$	$1.45 \times 10^{-14}$
Ring	$1.364 \times 10^{-2}$	$3.16 \times 10^{-3}$
Half ring	0.15401	$1.36 \times 10^{-3}$

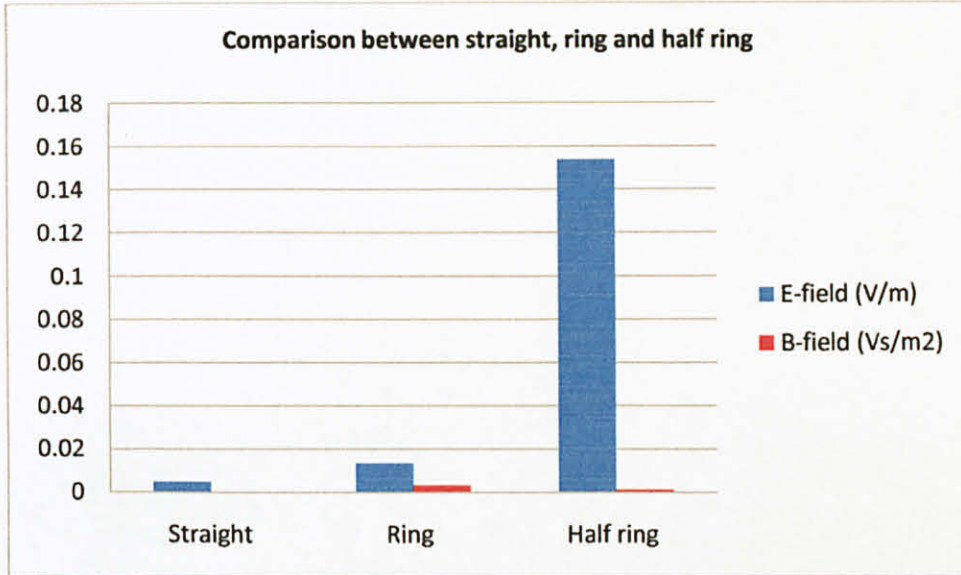


Figure 17: Result for three different configurations for simulation 4

From the result, we can conclude that the half ring antenna gave the greatest improvement on the amplification of electromagnetic wave. The signal is amplified at 3067% as compared to the straight shape and 1029% to the ring shape. This can be explained where the shape of the ring antenna gives greatest cancellation of magnetic field as the signal is outward to each other. While for the half ring antenna, the strong signals can be observed due to the higher concentration of electric field at the center of the antenna. This shows that the signal for the half ring antenna is more stable and capable enough to transmit strong electromagnetic wave and thus can be chosen for the best design antenna.



4.2 Preliminary Experiments

4.2.1 Experiment 1: Curvature of the EM transmitter

It should be recalled that the half ring transmitter had resulted to the highest magnification of the EM waves. This work promise deals with studying the effect of curvature on the magnification of the EM waves. With the same shape of antenna but different angle of curvature, this experiment is focusing on the total flux density that can be detected at receiver. A comparison between half ring and parabolic (curve) antenna is to be tested in this experiment.

Table 10: Setup of the experiment 1

SPECIFICATIONS	DETAILS
Model of function generator	Instek GFG-8250 A
Input waveform	Square wave
Transmitter	Aluminium rod
Detector	Bartington (Mag-03MSS100 sensor)
Length	0.974m
Diameter rod	0.009m

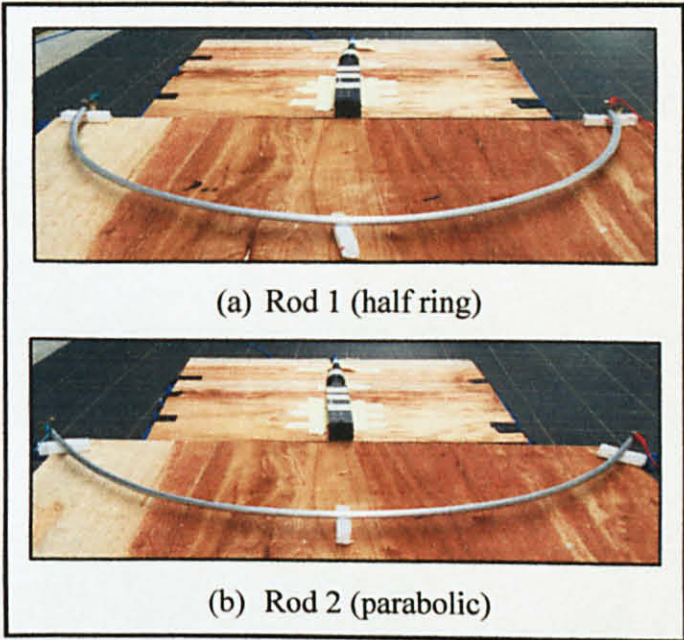


Figure 18: Two different curvatures of the antennas

The results are shown at Table 11 and represented in bar chart to see the comparison between the two rods. It should be noted that the length of the rod was kept constant and the voltage was fixed to 20V peak-to-peak.

Table 11: Result for experiment 1

TYPES OF ROD	MAGNETIC FIELD (T)
Rod 1 (half ring)	$7.23\text{E} \times 10^{-8}$
Rod 2 (parabolic)	$6.19 \times 10^{-8}$

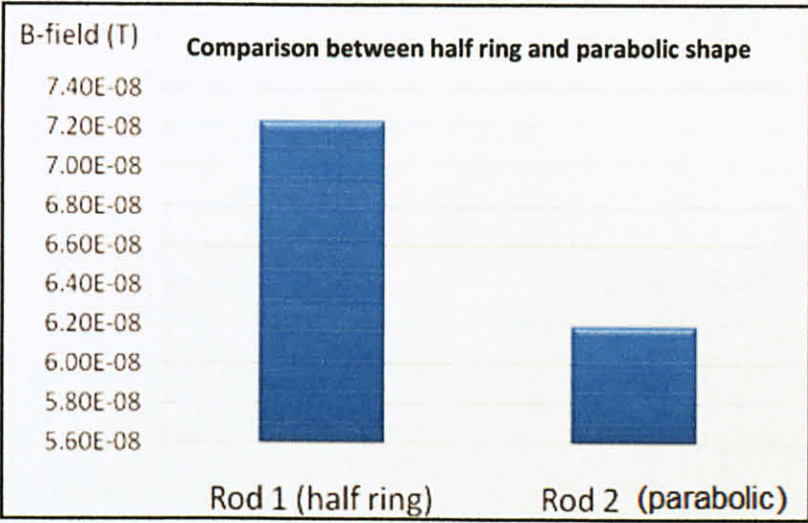


Figure 19: Bar chart for two types of rod with maximum magnetic field

From the bar chart, half ring produced higher magnetic field intensity with an increment of 16.80% as compared to the parabolic rod. This is due to the higher concentrating of magnetic field which produced from the center of the antenna. A wide curvature of parabolic antenna give affects to the transmitting electromagnetic wave since the signal propagation from one end to another end of the antenna is longer thus weaken the signal once it is arrived at the end point of the conductor.



**4.2.2 Experiment 2: Effect of Diameter/Cross Section of EM transmitter to the B-field**

The objective of this experiment is to investigate the significance of different thickness of aluminum which is varied to 0.38 mm, 1.00 mm, and 10.0 mm. We fixed the diameter of the half ring antenna at 620 mm and the length gives 974 mm after calculation. The supply voltage is 20V peak-to-peak with running frequency at 1 kHz. Table 12 shows the diagram for different thickness of aluminium.

Table 12: Different thickness of aluminium




DIAGRAM	THICKNESS
	0.38mm
	1.00mm
	10.00mm

Table 13: Result for experiment 2

DIAMETER ROD (mm)	B-field (T)
0.38	$6.41 \times 10^{-8}$
1.00	$6.69 \times 10^{-8}$
10.00	$7.23 \times 10^{-8}$



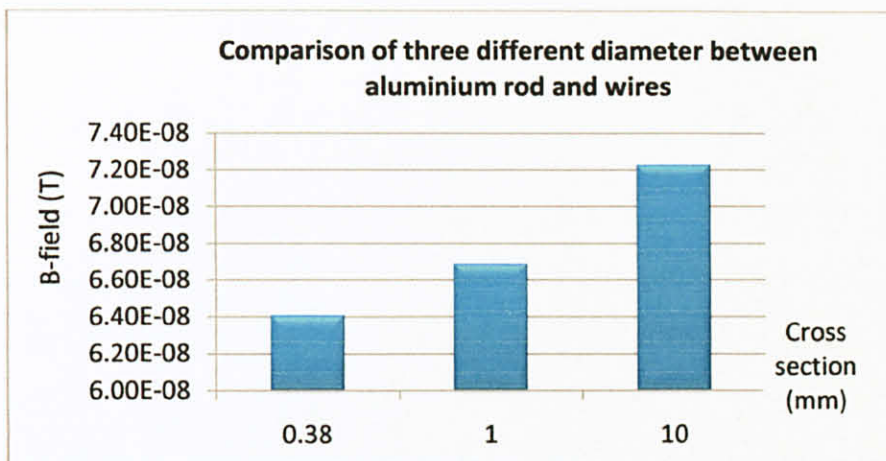


Figure 20: Bar chart for three types of different cross section

Based on the result obtained, the aluminium rod gives highest value of B-field with percentage of 12.79% as compared to the aluminium wire. We can see that there is no much difference of output result since aluminium wire has greater purity of conductivity that can produce higher EM wave as well. However, the thickness of the rod still affects the output result. The greater thickness of aluminium rod gives a medium for electrons to flow easily thus producing higher magnetic field. Below is an illustration shows different cross section between them to shows a clear picture on how the cross section affects the results.

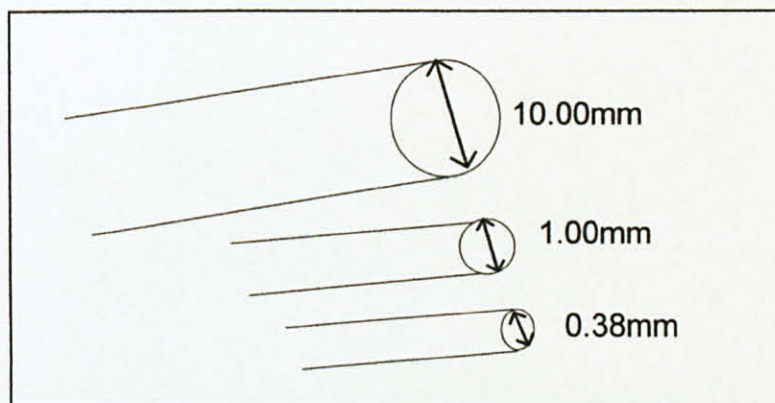


Figure 21: Illustration for different cross section of aluminium rod and wires

**4.2.3 Experiment 3: Effect of magnetic feeders to the strength of magnetic field**

In this experiment, we have two objectives to be implemented. The first objective is to observe the effectiveness of using magnetic feeders with a half ring antenna. The maximum number of magnetic feeders used in this experiment is five and it is placed equally divided over the length of the antenna. Secondly, we want to observe the magnitude of EM wave detected by fluxgate over the distance.

Table 14: Setup of the experiment 3

SPECIFICATIONS	DETAILS
Type of material	Aluminium
Length of material	974mm
Diameter of rod	10.0 mm
Diameter of half ring	620.0 mm
Types of magnetic feeder	Nickel Zinc Ferrites (20 winding)

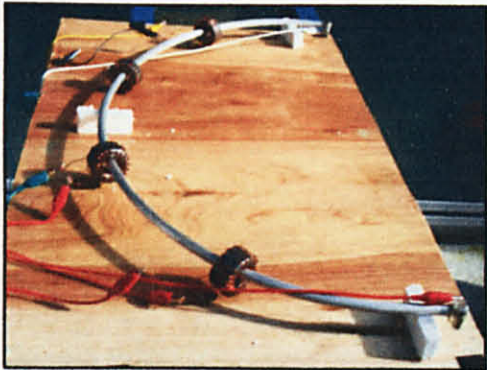


Figure 22: Half ring shape of aluminium rod as the transmitter

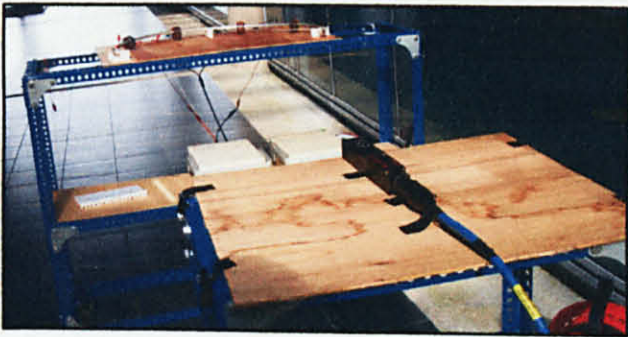


Figure 23: Setup diagram of the experiment 3



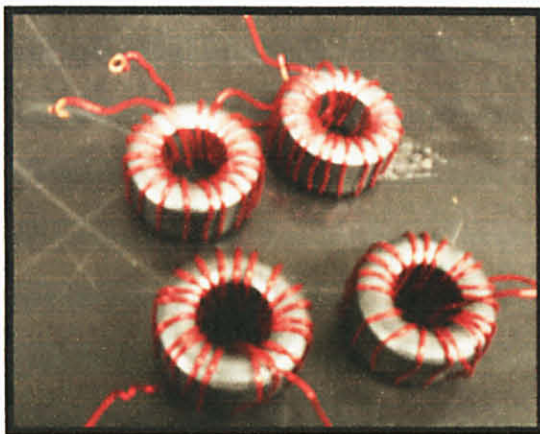


Figure 24: Nickel Zinc Ferrites with copper windings as magnetic feeder

Table 15: Requirements of magnetic feeders

SPECIFICATIONS	DETAILS
Code	D28
Material	Nickel Zinc Ferrites
Shape	Toroid
Inner diameter	0.0195m
Outer diameter	0.0370m
Height	0.0200m
Number of copper winding	20
Diameter of copper winding	0.0008m

Nickel zinc ferrite is one of the ferromagnetic materials which exhibit strong magnetic properties due to the fact that their magnetic moments tend to align readily along the direction of an external magnetic field [11]. When an alternating current is supplied to the copper windings, the copper windings will excite the feeders. The feeders which made from the nickel zinc ferrites will be induced once the current is flowing along the circulating winding. According to the Maxwell's Law, an electromagnetic radiation is consists of a magnetic field and electric field which are perpendicularly to each other. Therefore, the perpendicular electric field will be at the centre of the toroid thus amplifying the output of magnetic field which is already exists at the aluminium rod.



Below are the graphs plotted after obtaining the results for each number of toroid and Figure 26 is shown combining graph into one plotted axis.

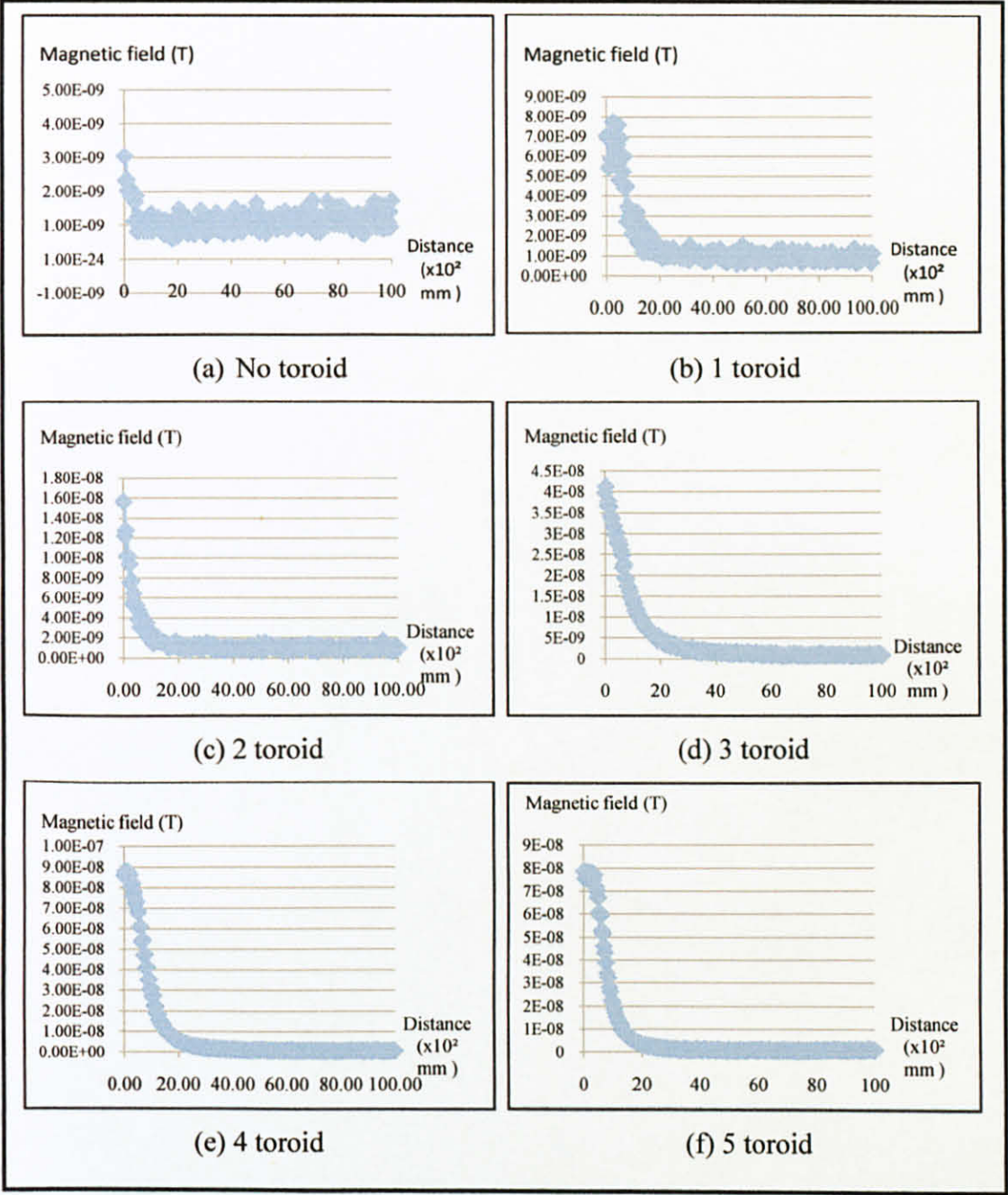


Figure 25: MVO of magnetic field over a distance

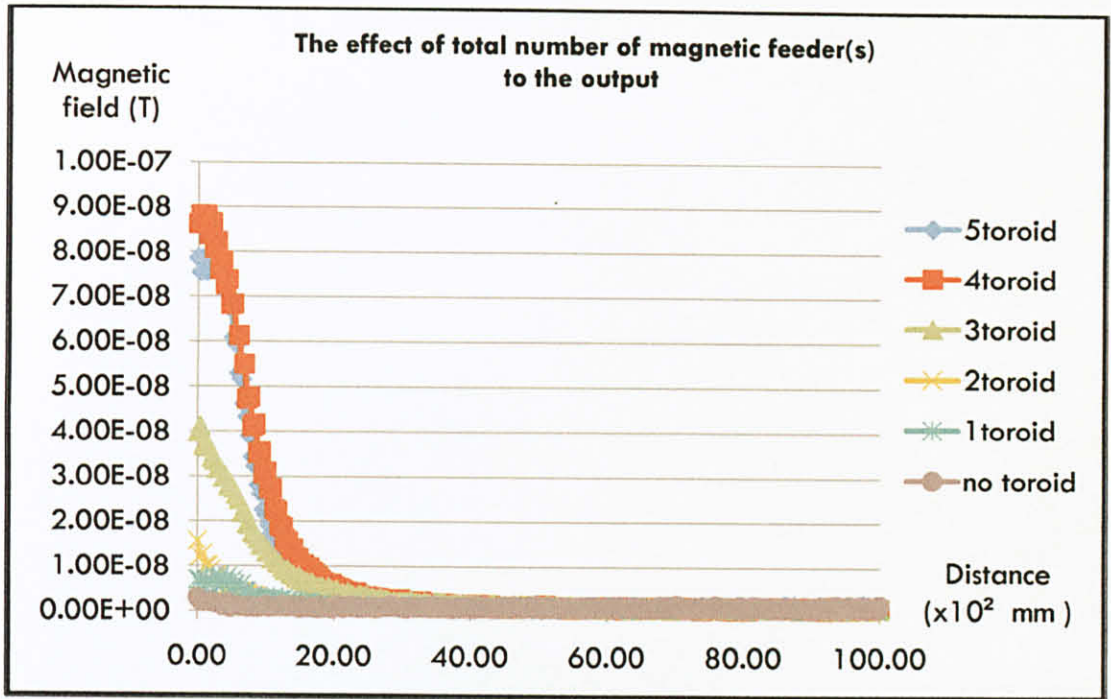


Figure 26: Magnitude versus offset for observation of curve transmitter

From the results obtained, we can see that the magnetic feeders can enhance the magnetic field of the antenna. It is proven that the utilization of magnetic feeders can generate strong magnetic field with 4 number of toroid gives the maximum amplification signal of 701%. Current in the coil windings induced higher magnetic field which produced from the feeders causing the detected signal to increase. By placing the detector away from the antenna, the magnitude of EM wave is decreasing and shows larger attenuation. In a real application, as the signal is transmitted over the seawater, the received signal contains three parts: the received signal due to the direct wave, which is the same as the signal received at the seabed case, the reflected wave, and the refracted wave. Since the reflected wave travels a longer distance in a seabed, a high attenuation occurs; the reflected signal is always weaker than the direct wave [21]. It is worth to note that using 5 magnetic feeders had resulted in a fall of the B-field. This is due to the fact that when more current is injected in the twin dipole, the resistance will increase and this had resulted in the fall of E-field and B-field due to Maxwell law [11].

#### 4.2.4 Experiment 4: Design and Development of Power Bridge Amplifier

This experiment is mainly to focused on the amplification current output generated by the power amplifier circuit which has been modified from the audio amplifier circuit. Power booster amplifiers can be easily designed using this device that provides a high current capability up to 3.5A and drive very low resistance loads obtaining an output power of more than 20W based on the bridge configuration. From the circuit, the TDA2005 needs a very low number of external components and has a very simple mounting system with no electrical isolation between the package and the heatsink which can be seen at Figure 27.

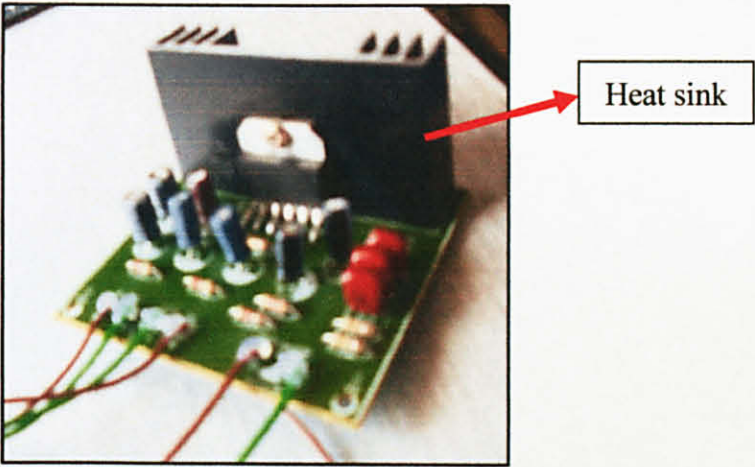


Figure 27: Circuit design of 20W power bridge amplifier

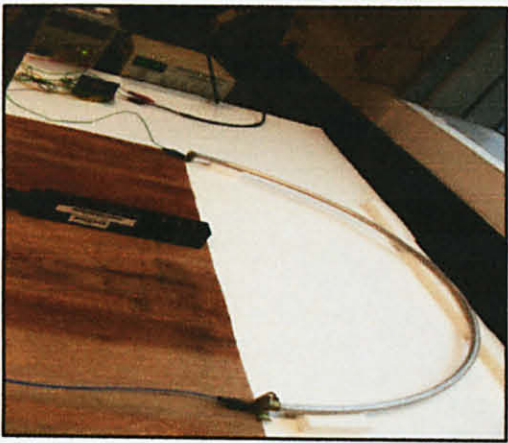


Figure 28: Setup of the experiment 4



The complete circuit diagram of the amplifier is designed by using P-Spice schematic. We have two terminals input; 12VDC input supply to power up the internal circuit and the signal input from the function generator to feed in electromagnetic wave to the antenna. The output of power amplifier circuit is then connected directly to the transmitter from the signal output as shown in figure below:

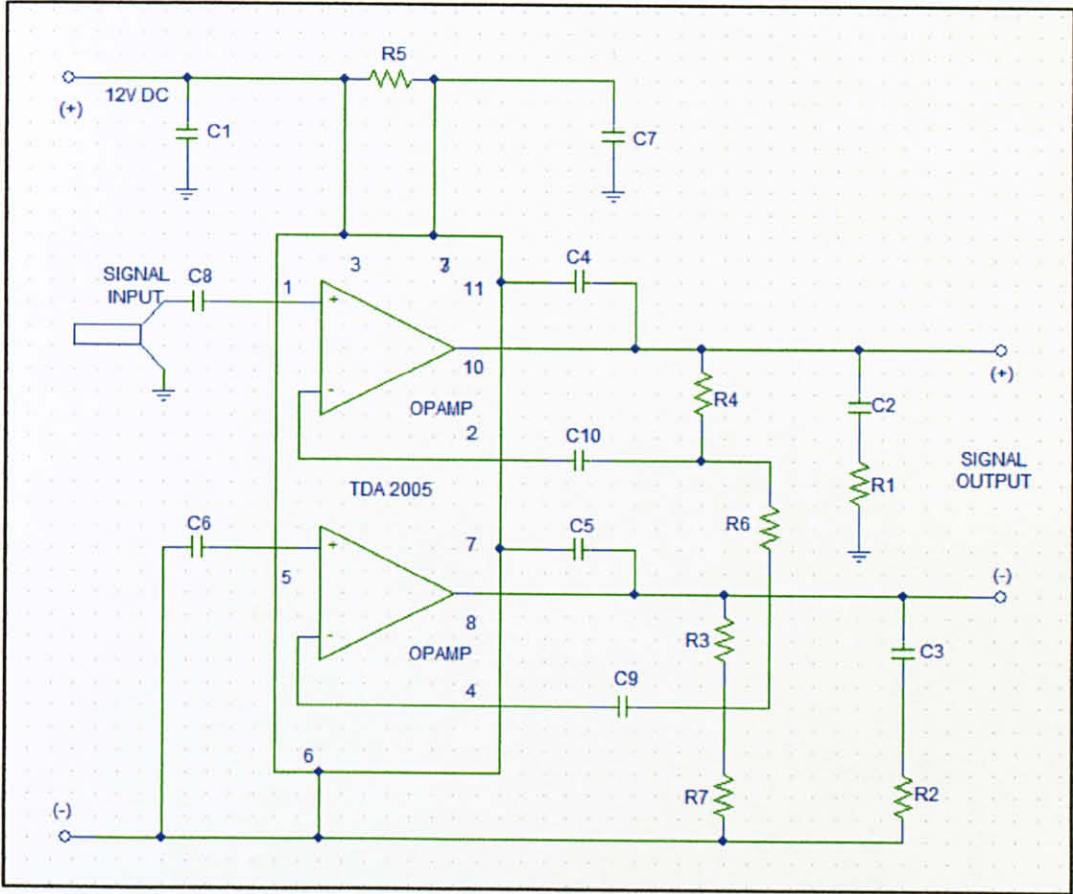


Figure 29: Circuit diagram of 20W power bridge amplifier

Below is the value for each resistor and capacitor used in this circuit:

$R1=R2=1\Omega$ ,  $R3=2K\Omega$ ,  $R4=1K\Omega$ ,  $R5=100K\Omega$ ,  $R6=R7=12\Omega$ ,  $C1=C2=C3=104$ ,  $C4=C5=100\mu F$ ,  $C6=2.2\mu F$ ,  $C7=10\mu F$ ,  $C8=2.2\mu F$ ,  $C9=C10=220\mu F$ , IC=TDA 2005

Table 16: Results for experiment 4

CONFIGURATION	B-field (T)
Without amplifier	$7.2 \times 10^{-8}$
With amplifier	$2.32 \times 10^{-7}$

From the result, the data is transferred into a bar chart to see a major difference between the two configurations. See Figure 30.

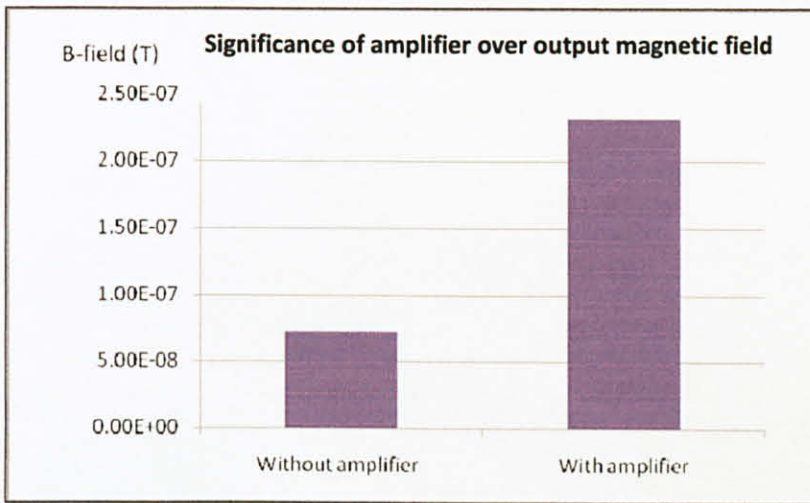


Figure 30: A comparison between two configurations of the antenna

We can see that the output signal is amplified at 220.89% when the bridge amplifier has been used to increase the output current thus increasing the output signal. It is proven successfully with the utilization of power bridge amplifier as one of the method to generate higher output waveform instead of combining magnetic feeders together with the antenna. This result implied with the simulation 2 which reported that as we increased the input power supply, the amplitude of magnetic field would be higher. In our case, other method is applied to generate higher input current since the input sources which is function generator has a minimum capability to produce higher amplitude input current signal.

**4.2.5 Experiment 5: Effect of Different Position Detector**

The next experiment is to determine the focus point of detector that gives an optimum output electromagnetic wave transmitted from the antenna. There are two configurations in placing the detector; zero displacement which is equivalent to the 'r' distance and double position from the first one which is equivalent to the '2r' distance. An illustration to this setup experiment is shown at figure below. For the first configuration, we placed the detector at three different configurations to detect highest possible value of magnetic field generated from the curve antenna.

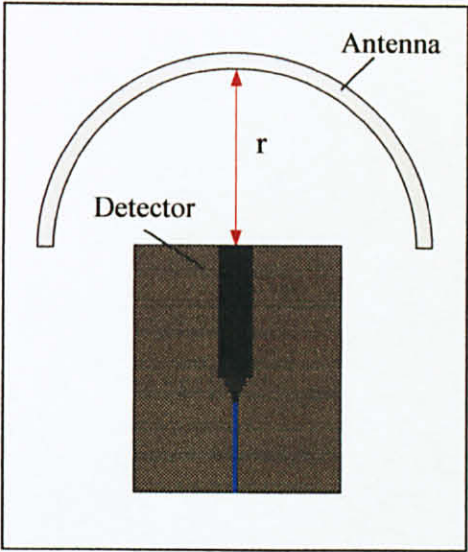


Figure 31: Detector at 'r' distance

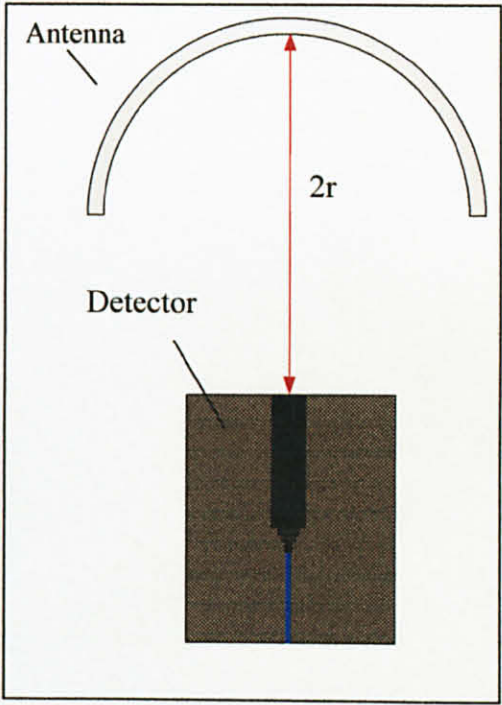
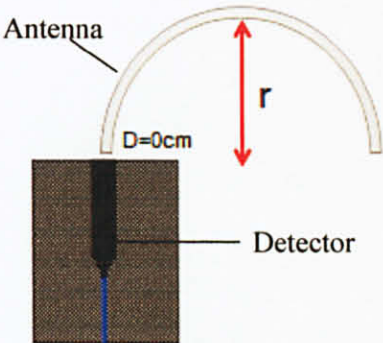
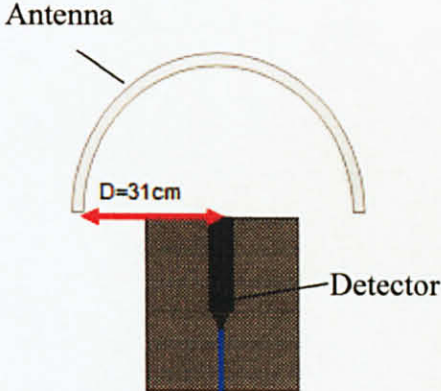
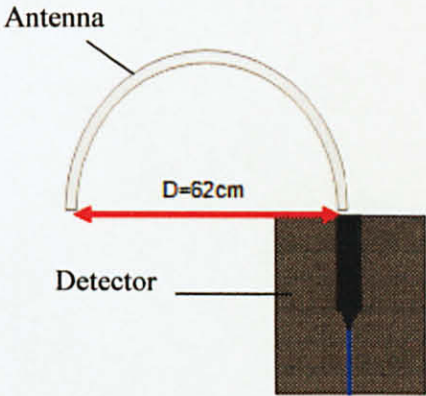


Figure 32: Detector at '2r' distance

Table 17 is shown the configuration of the setup experiment:



Table 17: Result of configuration 1 with an illustration of setup diagram

CONFIGURATION	SETUP DIAGRAM	B-FIELD (T) DETECTED
Series 1		$2.51 \times 10^{-7}$
Series 2		$1.09 \times 10^{-7}$
Series 3		$2.50 \times 10^{-7}$

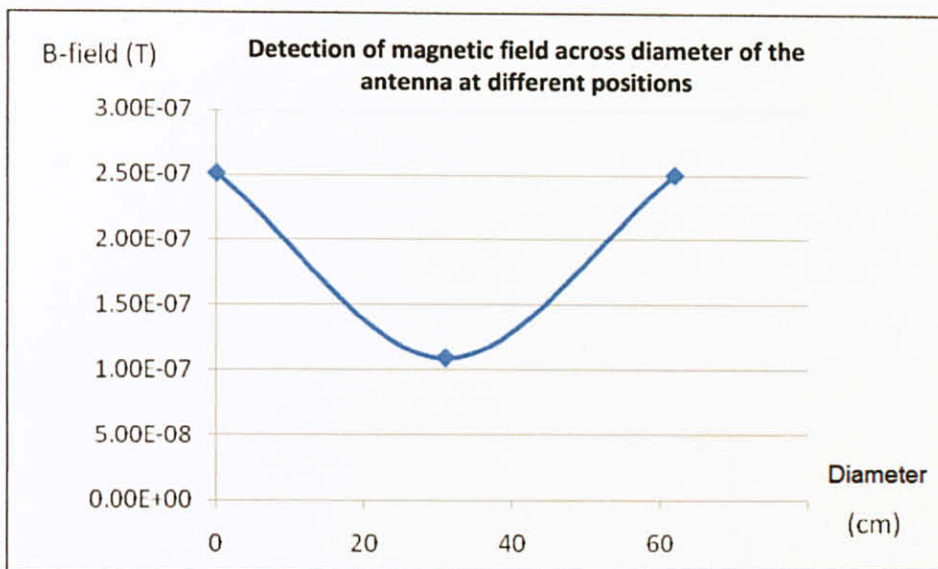


Figure 33: Result of configuration 1 for experiment 5

From the result, we can see that a minimum value of B-field is achieved when the detector is placed at the center of the curve antenna. We fed the injected current at both end of the antenna. Hence, there is more flux density and higher concentrating of the magnetic field at both ends as per shown in Figure 34 which gives an amplification signal of 31.58% as compared to the center position. All of these results were observed when we placed the detector next to the antenna.

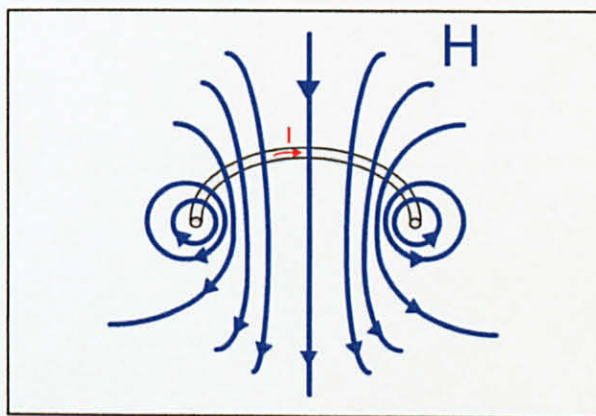
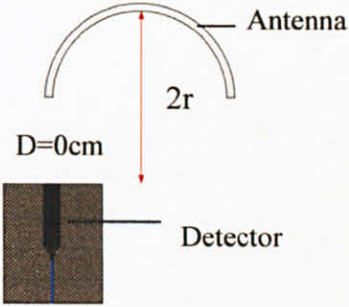
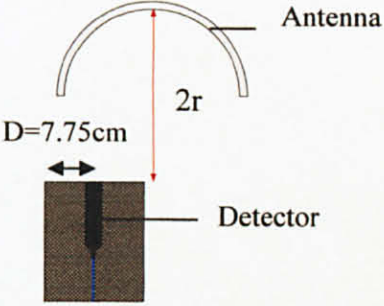
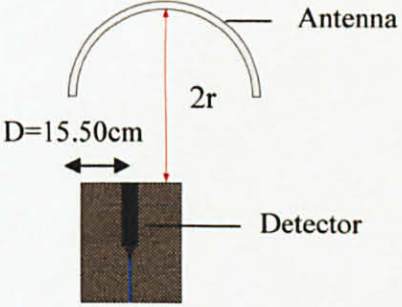
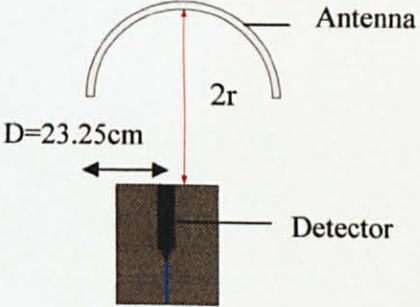


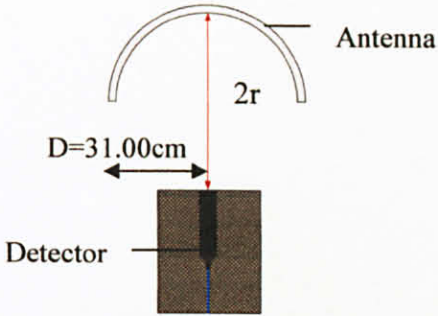
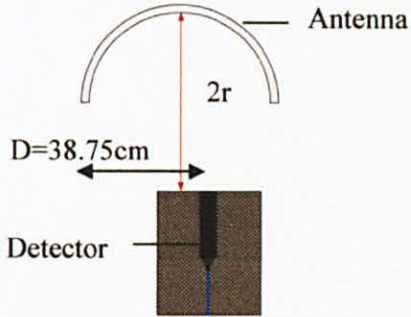
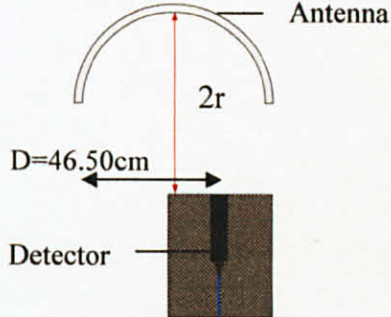
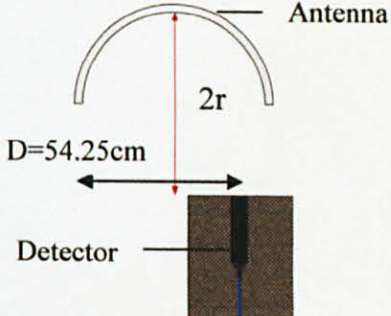
Figure 34: Pattern of magnetic field of curve antenna

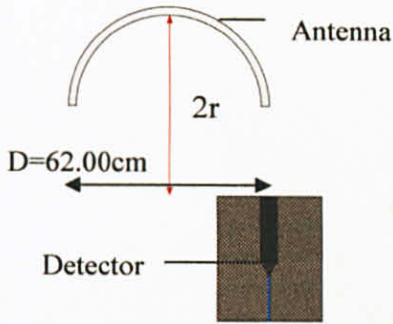
The results for configuration 2 are tabulated in Table 18.

Table 18: Result of configuration 2 with an illustration of setup diagram

CONFIGURATION	SETUP DIAGRAM	B-FIELD (T) DETECTED
Series 1		$2.51 \times 10^{-8}$
Series 2		$2.93 \times 10^{-8}$
Series 3		$3.74 \times 10^{-8}$
Series 4		$4.24 \times 10^{-8}$



<p>Series 5</p>	 <p>Antenna</p> <p><math>2r</math></p> <p><math>D=31.00\text{cm}</math></p> <p>Detector</p>	<p><math>4.36 \times 10^{-8}</math></p>
<p>Series 6</p>	 <p>Antenna</p> <p><math>2r</math></p> <p><math>D=38.75\text{cm}</math></p> <p>Detector</p>	<p><math>4.24 \times 10^{-8}</math></p>
<p>Series 7</p>	 <p>Antenna</p> <p><math>2r</math></p> <p><math>D=46.50\text{cm}</math></p> <p>Detector</p>	<p><math>3.74 \times 10^{-8}</math></p>
<p>Series 8</p>	 <p>Antenna</p> <p><math>2r</math></p> <p><math>D=54.25\text{cm}</math></p> <p>Detector</p>	<p><math>2.93 \times 10^{-8}</math></p>

Series 9		$2.51 \times 10^{-8}$
----------	---	-----------------------

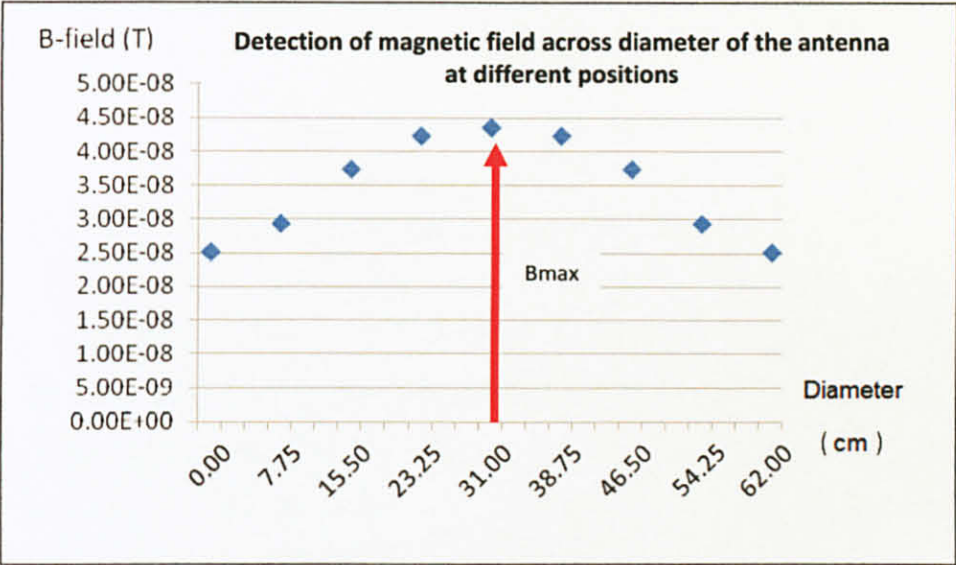


Figure 35: Result of configuration 2 for experiment 5

From the plotted graph, we can see that the focus point that gives higher concentration of magnetic flux density that gives amplification of 73.71% improvement is positioning at the center of half ring antenna. However, the output signal has been reduced when the detector is placed at both end of the curve antenna. This result is inversed from previous result where the output of magnetic field is lowered at the center of curve antenna. As we increased the position between the detector and the transmitter, we can eventually see a major impact on the cancellation of EM wave from both end of the curve antenna. Thus, this result is validated with respect to the simulation result of Simulation 3.

**4.2.6 Experiment 6: Effect of solenoid to the output magnetic field**

This experiment is intended to improve a current design of the antenna. An inductor can store magnetic energy in the volume comprising the inductors. A typical example of an inductor is a coil consisting of multiple turns of wire wound in a helical geometry around a cylindrical core, as shown in Figure 36.

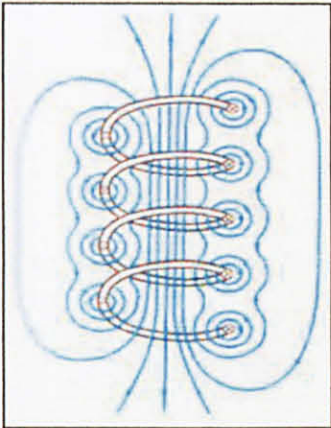


Figure 36: Magnetic field lines of a loosely wound solenoid [11]

This form of winding is represented as a loosely wound solenoid. By using this concept, we construct the antenna with a solenoid of copper wire to induce higher magnetic flux density. We make a comparison between curve antenna with windings and also twin curve antenna with two set of windings. An illustration to the setup of this experiment is demonstrated at Figure 37 and Figure 38.

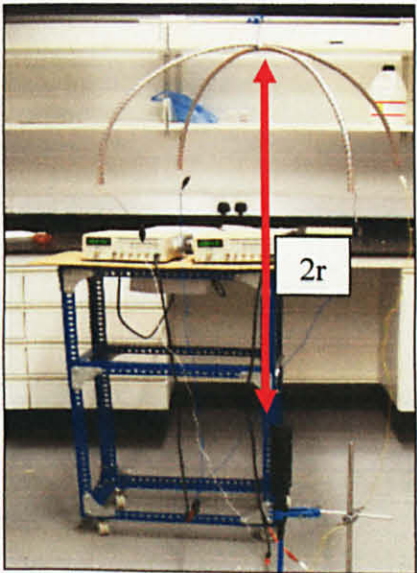
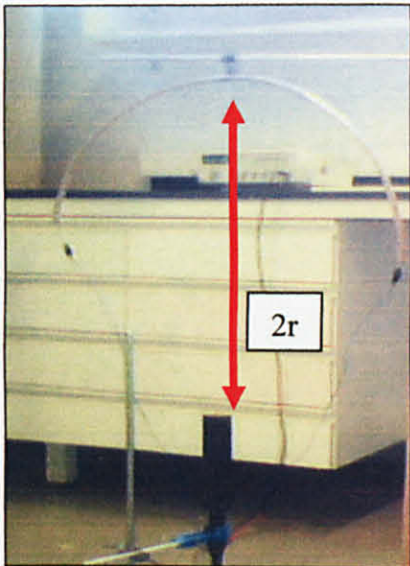


Figure 37: A curve antenna with windings      Figure 38: Twin curve antenna with two set of windings



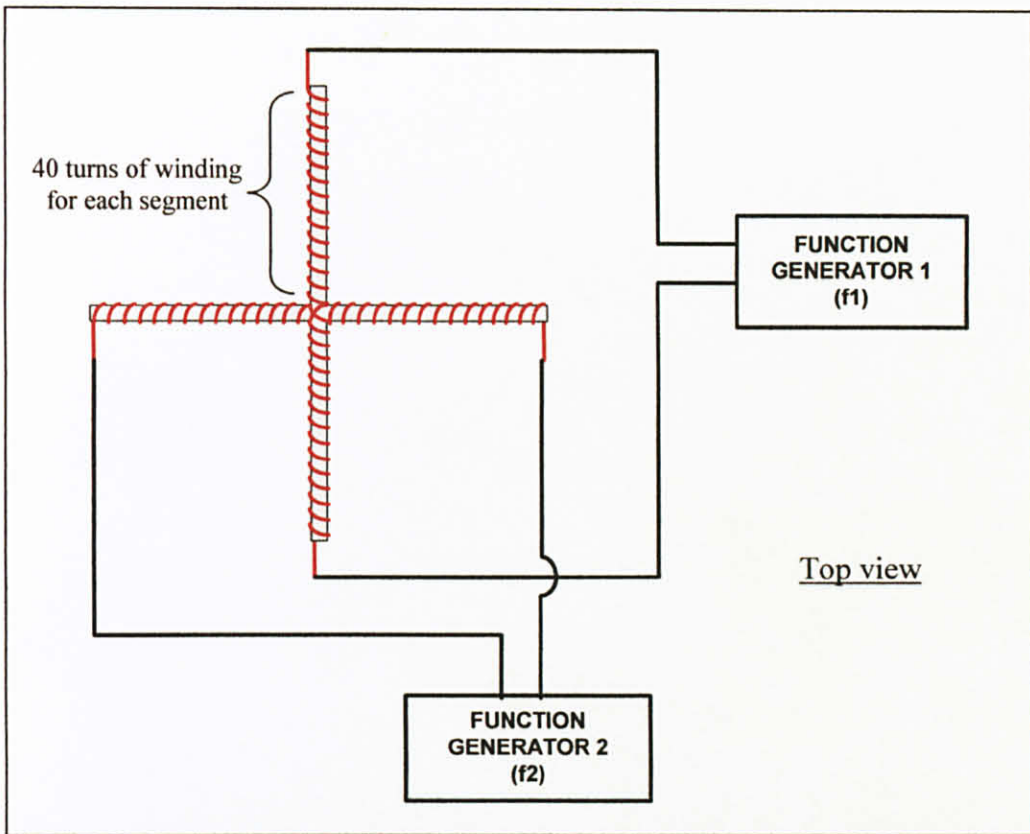


Figure 39: Setup of the experiment 6

For the twin curve antenna, the design is originated from the two curves of half ring aluminium rods which is centered at the middle and also combined to form 3-dimension of hemisphere shape as shown in Figure 40. We fixed the number of windings at 40 turns for each segment of half-curve antenna with a constant separation between them. The power source of the antenna must be limited to the external supply only which is to the windings. As a result, the current will not be flowing along the conductor. If a current is flowing directly to the conductor, it will circulate within the same point of the antenna which can caused a short circuit.

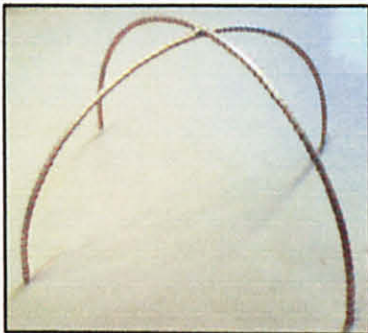


Figure 40: Twin curve aluminium rod

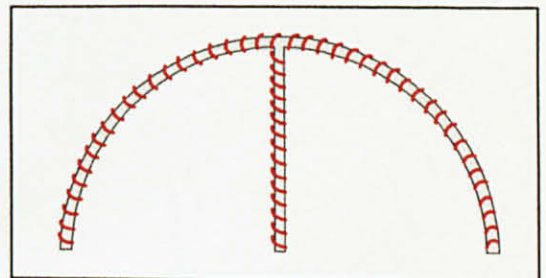


Figure 41: Front view of twin curve antenna

Table 19: Result of the experiment 6

CONFIGURATION	MAGNETIC FIELD (T)
1 curve antenna + winding	$9.83 \times 10^{-8}$
Twin curve antenna + 2 windings	$1.93 \times 10^{-7}$

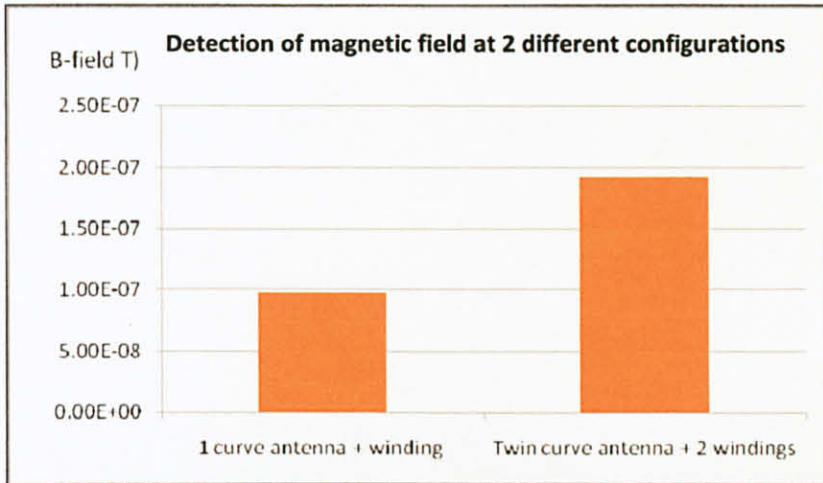


Figure 42: Bar chart for two different configurations

From the result, if we make a comparison between the curve antenna without winding and the curve antenna with a winding, we can see that the signal is amplified with an increment signal of 125.46%. This amplification is higher with the twin curve antenna which gives greatest result output with percentage increment of 96.34% as compared to the curve antenna with windings and 342.66% with a comparison to the previous design antenna, which is the curve antenna without windings.

**4.2.7 Experiment 7: Prototype design testing in scaled tank filled with salt water**

The goal of this experiment is to testing the final prototype design in salt water. The experimental setup consisted of a large water tank is shown in Figure 45. The tank had a surface area of 1.82 m by 0.91 m and depth of 0.61 m. A conductive environment was created by filling the entire tank with saltwater. A resistivity of  $1.18\Omega\text{m}$  is measured by using the resistivity meter. The twin curve antenna was used as source and the inline configuration were used to allocate the source and the receiver where basically the separation distance between them is parallel to the distance of the antenna [22].

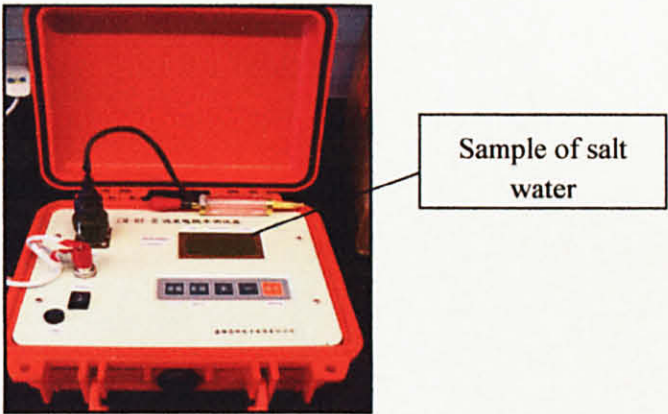


Figure 43: Resistivity meter

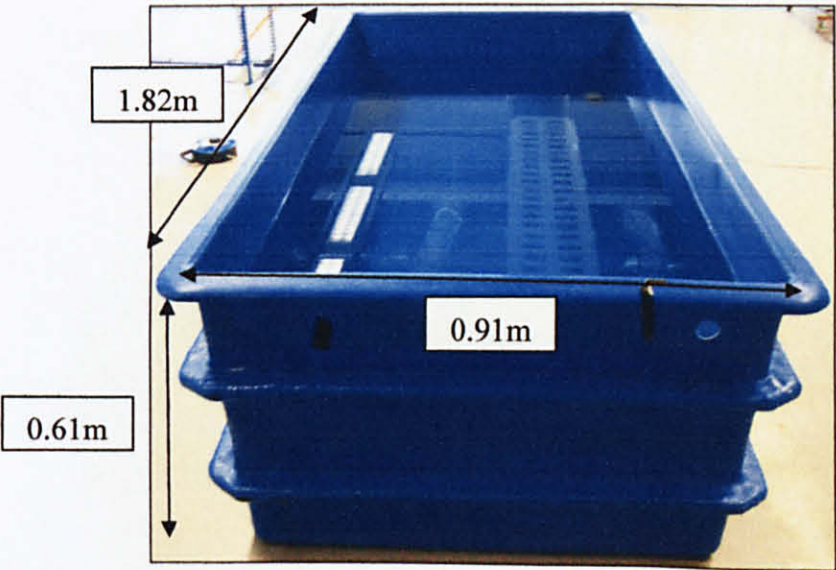


Figure 44: Scaled tank filled with saltwater



The antenna was clinging to the upper part of the trolley and it will be moved together with the trolley along the side of the tank. As mentioned in literature review, the detector is positioned at the seafloor. Hence, to simulate the SBL application, we placed the detector on the floor of the tank.



Figure 45: Setup of the experiment 7

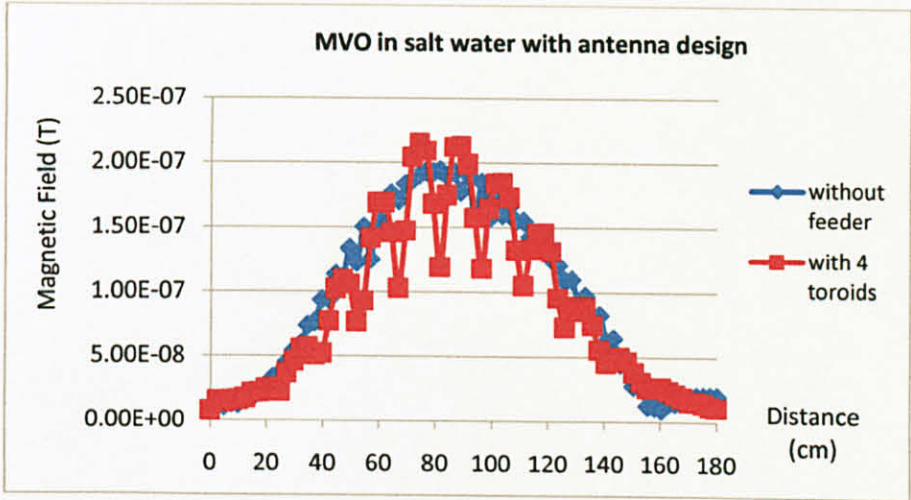


Figure 46: Result of the experiment 7

From the graph plotted above, it shows that the magnetic field as a function of source receiver offset. The red color curve shows that the magnetic field response to the toroids inserted into the antenna and some distortion were observed at the output waveform. This is due to the hysteresis where difficulty of aligning the magnetic domains in the toroids. The antenna has some limitation of receiving input current signal where the size of the antenna must be parallel with the wavelength being transmitted.

Below is the table of summary for result prototype design:

Table 20: Summary of the prototype design

CONFIGURATION	DETAILS		IMPROVEMENT
1	Curve antenna without winding	+ Curve antenna with winding	<b>125.46%</b>
2	Curve antenna without winding	+ Twin curve antenna with winding	<b>342.66%</b>
3	Curve antenna without winding	+ Twin curve antenna with winding and 4 toroids	<b>388.53%</b>

## CHAPTER 5

### CONCLUSION AND RECOMMENDATIONS

#### 5.1 Conclusion

After performing several preliminary experiments, we can see that the development of powerful antenna for hydrocarbon exploration is achieved. A twin curve antenna with magnetic feeders was successfully invented. This invention is coming from the scratch idea in development of powerful antenna. The results from the experiments had shown impressive output readings. An increased in the magnetic field is achieved when we increased the input sources from 5V to 20V and it is amplified at 300.00%. We increased the length of the transmitter and also we changed the shape of the antenna. It is concluded that the half ring gives greatest improvement on the amplification of EM wave. The signal is amplified at 3067.09% as compared to the straight shape and 1029.11% to the ring shape. A further investigation by varying the diameter and the curvatures of the antenna which shows that aluminium rod gives highest value of magnetic field with percentage of 12.79% as compared to the aluminium wire. The antenna with half ring shape is shown very promising results as compared to the parabolic shape. Moreover, the utilization of magnetic feeder enhanced the magnetic field intensity of the dipole antenna with 4 number of toroid gives maximum amplification of 700.88%. Next, by adding bridge power amplifier circuit to the antenna has boosted up the input current signal by 220.89%. Relative to the current design, a twin curve antenna is developed where the effect of interference wave has been included to obtained best output result. The final prototype design has been tested in salt water which gives accurate output result and based on the findings, it is confirmed that the magnetic feeders can be used to enhance the electromagnetic wave by percentage increment of 388.53%. However, there is a constraint to include the amplifier in the current design since the antenna itself has some capability to received high power input current.



5.2 Recommendations

For the next planning future work, it is recommended to conduct the experiment which includes the pre-amplifier circuit and the toroids together. The antenna needs to be up-scaled as comparable to the size of the scaled tank so that it could drive more input current signal. Here the scaled tank has to be enlarged and so that the scaled factor is decrease. Studies must also be conducted to change the frequency which has to be reduced with the increasing size of the scaled tank. Without changing the current situation, a very high saturation of electromagnetic wave will be circulating along the antenna and limits them to go further. Other recommendation for this project is to further investigate the characteristic of the antenna by varying the resistivity of salt water and make a comparison between them in obtaining accurate readings. Moreover, the frequency of the input current signal can be varied at several readings. The lower the frequency, the higher the electromagnetic wave can penetrate through the salt water. Besides that, we can also investigate the impact of placing the feeders at different places. Instead of putting the feeders in the middle of the antenna, we can actually placing them at the center and the end of the antenna as shown in figure below:

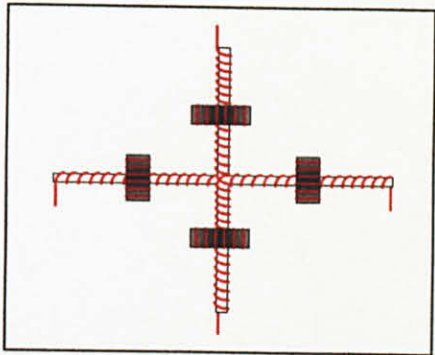


Figure 47: Middle position of magnetic feeders based on the existing design

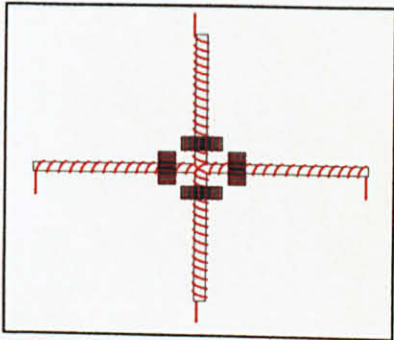


Figure 48: Center position of magnetic feeders

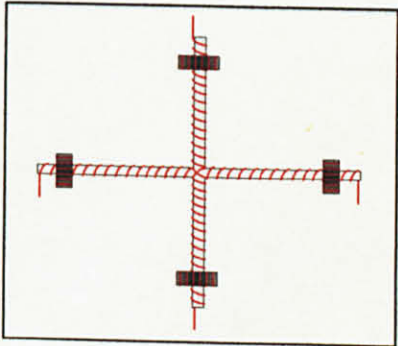


Figure 49: End position of magnetic feeders

## REFERENCES

- [1] Halfdan Carstens , 'The same PRINCIPLE as in borehole logging', GEO Expro, June 2004
- [2] Rocksource, 'EM in Exploration' from <http://www.rocksource.com>
- [3] Anwar Bhuiyan, Tor Wicklund, and Stale Johansen, 'High-resistivity anomalies at Modgunn arch in the Norwegian Sea', *first break* volume 24, January 2006
- [4] StatoilHydro , 'About Seabed logging' from <http://www.statoilhydro.com>
- [5] T.Eidesmo,S.Ellingsrud,L.M.MacGregor,S. Constable, M.C. Sinha, S.Johansen, F.F. Kong and H.Weterdahl, 'Sea Bed Logging (SBL), a new method for remote and direct identification of hydrocarbon filled layers in deepwater areas', *first break* volume 20, 3 March 2002
- [6] Bhuiyan, A.H., Wicklund, T.A, and Johansen, S.E [2005] Geophysical characterization of subseafloor strata of Modgunn Arch from SBL data. 67<sup>th</sup> EAGE Conference, Madrid,Spain, Extended Abstracts.
- [7] Nur Intan Baizura, 'Development of Powerful Twin Antenna for Hydrocarbon Exploration', Degree Thesis 2009, Universiti Teknologi PETRONAS
- [8] L.O Loseth, H.M. Pedersen, T.Schaug-Pettersen, S.Ellingsrud, and T.Eidesmo, 'The first test of the Seabed Logging method' *Submitted to Journal of Applied Geophysics*
- [9] F.N. Kong and H. Westerdahl, 'Excitation of a Long Wire Antenna', Tenth International Conference on Ground Penetrating Radar, 21-24 June 2004.
- [10] Rune Mittet and Tor Schaug-Pettersen, 'Shaping optimal transmitter waveforms for marine CSEM surveys' *Geophysics*, Vol.37 ,No.3, May June 2008

- [11] Electromagnetics for Engineers , *Fawwaz T.Ulaby*
- [12] 'Electromagnetic waves' from [http://www.amazingrust.com/Experiments/background\\_knowledge/Spectroscopy.html](http://www.amazingrust.com/Experiments/background_knowledge/Spectroscopy.html)
- [13] 'Amperes circuital Law' from [http://en.wikipedia.org/wiki/Amperes\\_circuital\\_law](http://en.wikipedia.org/wiki/Amperes_circuital_law)
- [14] 'Interference' from <http://en.wikipedia.org/wiki/Interference>
- [15] 'A brief history from phased array testing' from <http://www.olympus-ims.com>
- [16] 'Skin depth' from <http://www.fas.harvard.edu>
- [17] B. K. Bhattacharyya, 'Input Resistances of Horizontal Electric and Vertical Magnetic Dipoles Over a Homogenous Ground', IEEE Transactions on Antennas and Propagation, May 1963.
- [18] Ronold W. P. King, 'Antennas in Material Media Near Boundaries with Application to Communication and Geophysical Exploration, Part I: The Bare Metal Dipole', IEEE Transactions on Antennas and Propagation, Vol. AP-34, No.4, April 1986.
- [19] Ronold W. P. King, 'Antennas in Material Media Near Boundaries with Application to Communication and Geophysical Exploration, Part II: The Terminated Insulated Antenna, IEEE Transactions on Antennas and Propagation, Vol. AP-34, No.4, April 1986.
- [20] John A. Bell, 'Method of producing a continuously processed copper rod', Patented Oct. 31, 1967
- [21] F. N. Kong, Harald Westerdahl, Svein Ellingsrud, Terje Eidesmo and Stale Emil Johansen, 'Seabed logging: A possible direct hydrocarbon indicator for deepsea prospect using EM energy', Oil and Gas Journal, 13 May 2002.



- [22] L.O Loseth, H.M. Pedersen, T. Schaug-Pettersen, S. Ellingsrud, T. Eidesmo, 'A scaled experiment for the verification of the Seabed Logging method' , Journal of Applied Geophysics 64 (2008) 47-55.

## APPENDICES

**APPENDIX A**  
**DATA FOR EXPERIMENT 3**



Distance (cm)	No toroid	1 toroid	2 toroid	3 toroid	4 toroid	5 toroid
0.00	3.05E-09	7.04E-09	1.57E-08	3.98E-08	8.62E-08	7.87E-08
0.40	2.33E-09	6.92E-09	1.22E-08	4.12E-08	8.82E-08	7.55E-08
0.80	2.35E-09	5.43E-09	1.28E-08	3.68E-08	8.51E-08	7.85E-08
1.20	2.04E-09	6.88E-09	1.02E-08	3.78E-08	8.81E-08	7.56E-08
1.61	2.06E-09	5.86E-09	1.01E-08	3.65E-08	8.39E-08	7.84E-08
2.01	2.09E-09	7.12E-09	9.39E-09	3.42E-08	8.64E-08	7.69E-08
2.41	1.88E-09	7.73E-09	7.56E-09	3.35E-08	8.07E-08	7.80E-08
2.81	1.90E-09	5.70E-09	7.76E-09	3.17E-08	8.23E-08	7.82E-08
3.21	1.83E-09	7.66E-09	5.42E-09	3.18E-08	7.60E-08	7.48E-08
3.61	1.13E-09	6.24E-09	6.45E-09	2.97E-08	7.78E-08	7.72E-08
4.02	1.69E-09	6.57E-09	5.37E-09	3.03E-08	7.26E-08	7.19E-08
4.42	1.88E-09	7.59E-09	5.33E-09	2.78E-08	7.38E-08	7.02E-08
4.82	8.05E-10	4.82E-09	5.27E-09	2.85E-08	6.82E-08	6.74E-08
5.22	1.10E-09	6.92E-09	3.83E-09	2.73E-08	6.83E-08	6.08E-08
5.62	1.18E-09	6.01E-09	4.69E-09	2.60E-08	6.12E-08	5.94E-08
6.02	1.22E-09	5.24E-09	3.07E-09	2.49E-08	6.13E-08	5.29E-08
6.43	9.27E-10	6.00E-09	4.29E-09	2.19E-08	5.39E-08	5.16E-08
6.83	9.93E-10	4.41E-09	3.95E-09	2.26E-08	5.50E-08	4.61E-08
7.23	8.41E-10	4.51E-09	3.82E-09	1.94E-08	4.72E-08	4.32E-08
7.63	9.52E-10	2.70E-09	3.68E-09	1.92E-08	4.76E-08	3.90E-08
8.03	8.67E-10	3.47E-09	2.75E-09	1.75E-08	4.11E-08	3.43E-08
8.43	8.29E-10	2.99E-09	3.50E-09	1.71E-08	4.15E-08	3.23E-08
8.84	8.51E-10	3.30E-09	2.14E-09	1.61E-08	3.51E-08	2.80E-08
9.24	1.06E-09	2.98E-09	2.83E-09	1.46E-08	3.54E-08	2.62E-08
9.64	1.05E-09	2.10E-09	2.34E-09	1.47E-08	3.05E-08	2.26E-08
10.04	1.35E-09	3.16E-09	2.03E-09	1.31E-08	3.10E-08	2.15E-08
10.44	8.21E-10	2.71E-09	2.37E-09	1.33E-08	2.73E-08	1.92E-08
10.84	1.07E-09	2.64E-09	1.48E-09	1.16E-08	2.74E-08	1.73E-08
11.24	9.76E-10	3.20E-09	2.30E-09	1.19E-08	2.27E-08	1.54E-08
11.65	1.01E-09	1.69E-09	1.77E-09	1.08E-08	2.23E-08	1.41E-08
12.05	9.62E-10	2.69E-09	1.99E-09	1.05E-08	1.91E-08	1.31E-08
12.45	1.23E-09	2.67E-09	1.72E-09	9.71E-09	1.87E-08	1.18E-08
12.85	1.15E-09	2.03E-09	1.92E-09	9.05E-09	1.60E-08	1.17E-08
13.25	9.93E-10	2.43E-09	1.65E-09	9.22E-09	1.54E-08	9.68E-09
13.65	1.14E-09	1.18E-09	1.63E-09	8.30E-09	1.38E-08	9.39E-09
14.06	1.08E-09	2.30E-09	1.66E-09	8.05E-09	1.38E-08	8.13E-09
14.46	1.03E-09	1.89E-09	1.57E-09	7.38E-09	1.21E-08	7.83E-09
14.86	7.34E-10	1.37E-09	1.45E-09	7.77E-09	1.18E-08	7.39E-09
15.26	1.15E-09	1.65E-09	1.51E-09	7.16E-09	1.04E-08	6.85E-09
15.66	8.76E-10	1.22E-09	1.20E-09	6.71E-09	1.05E-08	6.94E-09
16.06	9.35E-10	2.14E-09	1.28E-09	6.45E-09	9.05E-09	5.96E-09
16.47	8.48E-10	1.85E-09	1.07E-09	6.17E-09	9.78E-09	6.20E-09
16.87	8.68E-10	1.17E-09	1.18E-09	6.35E-09	8.87E-09	5.22E-09
17.27	1.00E-09	1.25E-09	1.37E-09	5.50E-09	8.33E-09	5.15E-09



17.67	6.09E-10	1.51E-09	1.25E-09	5.40E-09	7.73E-09	4.82E-09
18.07	1.15E-09	1.75E-09	1.35E-09	5.46E-09	6.96E-09	4.38E-09
18.47	8.66E-10	1.10E-09	1.21E-09	5.38E-09	6.40E-09	4.29E-09
18.88	8.61E-10	1.34E-09	1.66E-09	4.45E-09	6.08E-09	3.91E-09
19.28	8.20E-10	1.16E-09	1.13E-09	5.38E-09	6.05E-09	4.00E-09
19.68	6.66E-10	1.24E-09	1.31E-09	4.72E-09	6.02E-09	3.52E-09
20.08	8.48E-10	1.16E-09	1.04E-09	4.44E-09	5.58E-09	3.17E-09
20.48	1.48E-09	1.33E-09	1.23E-09	4.71E-09	5.17E-09	3.19E-09
20.88	1.02E-09	8.67E-10	1.39E-09	3.90E-09	5.15E-09	3.20E-09
21.28	8.16E-10	1.17E-09	1.05E-09	4.09E-09	4.73E-09	3.10E-09
21.69	9.71E-10	1.21E-09	1.29E-09	3.64E-09	4.50E-09	2.72E-09
22.09	1.08E-09	1.05E-09	1.12E-09	4.27E-09	4.33E-09	2.66E-09
22.49	9.17E-10	1.38E-09	9.63E-10	3.89E-09	4.10E-09	2.90E-09
22.89	1.29E-09	9.53E-10	1.12E-09	3.55E-09	4.19E-09	2.85E-09
23.29	1.09E-09	1.03E-09	1.11E-09	3.10E-09	4.17E-09	2.64E-09
23.69	7.54E-10	1.22E-09	1.22E-09	3.63E-09	3.65E-09	2.81E-09
24.10	7.66E-10	1.04E-09	8.05E-10	3.45E-09	3.36E-09	2.35E-09
24.50	9.63E-10	1.08E-09	1.01E-09	3.39E-09	3.33E-09	2.18E-09
24.90	1.07E-09	1.40E-09	1.19E-09	3.53E-09	3.31E-09	2.24E-09
25.30	8.90E-10	9.46E-10	1.11E-09	2.79E-09	2.85E-09	1.94E-09
25.70	1.03E-09	9.79E-10	1.38E-09	3.17E-09	3.17E-09	2.35E-09
26.10	7.25E-10	1.22E-09	1.26E-09	2.76E-09	3.02E-09	2.12E-09
26.51	8.31E-10	1.02E-09	1.09E-09	2.80E-09	3.06E-09	2.01E-09
26.91	1.05E-09	9.94E-10	1.12E-09	3.08E-09	2.87E-09	2.05E-09
27.31	1.05E-09	1.00E-09	1.44E-09	2.66E-09	2.66E-09	1.57E-09
27.71	1.05E-09	9.11E-10	9.79E-10	2.72E-09	2.57E-09	2.06E-09
28.11	1.05E-09	9.33E-10	1.11E-09	2.44E-09	2.58E-09	1.88E-09
28.51	1.44E-09	1.11E-09	8.85E-10	1.97E-09	2.34E-09	1.87E-09
28.92	1.15E-09	8.93E-10	1.01E-09	2.29E-09	2.24E-09	1.69E-09
29.32	1.04E-09	9.10E-10	1.13E-09	1.99E-09	2.16E-09	1.66E-09
29.72	1.08E-09	1.29E-09	1.16E-09	2.30E-09	2.73E-09	1.56E-09
30.12	9.62E-10	9.66E-10	1.49E-09	2.12E-09	1.98E-09	1.82E-09
30.52	7.06E-10	9.05E-10	1.34E-09	2.10E-09	2.22E-09	1.57E-09
30.92	9.53E-10	7.74E-10	1.42E-09	2.23E-09	1.76E-09	1.80E-09
31.32	1.10E-09	1.53E-09	1.09E-09	2.77E-09	2.08E-09	1.65E-09
31.73	9.58E-10	1.09E-09	1.05E-09	2.04E-09	2.02E-09	1.36E-09
32.13	1.15E-09	1.23E-09	1.16E-09	2.07E-09	1.81E-09	1.59E-09
32.53	1.05E-09	9.95E-10	8.38E-10	1.96E-09	2.08E-09	1.28E-09
32.93	9.62E-10	1.17E-09	1.37E-09	1.64E-09	2.31E-09	1.03E-09
33.33	1.05E-09	1.02E-09	1.13E-09	2.25E-09	1.68E-09	1.23E-09
33.73	9.03E-10	1.10E-09	8.09E-10	1.88E-09	1.87E-09	1.51E-09
34.14	8.86E-10	1.17E-09	1.04E-09	1.85E-09	1.90E-09	1.50E-09
34.54	1.37E-09	9.13E-10	8.91E-10	1.47E-09	1.80E-09	1.64E-09
34.94	1.06E-09	1.21E-09	9.00E-10	2.18E-09	1.62E-09	1.21E-09
35.34	8.40E-10	1.02E-09	9.28E-10	2.15E-09	1.52E-09	1.77E-09



35.74	9.50E-10	9.03E-10	9.93E-10	1.98E-09	1.94E-09	1.10E-09
36.14	1.12E-09	8.22E-10	9.32E-10	2.09E-09	1.71E-09	1.39E-09
36.55	8.63E-10	9.06E-10	7.99E-10	1.69E-09	1.82E-09	8.45E-10
36.95	8.55E-10	7.17E-10	1.04E-09	1.56E-09	1.42E-09	1.11E-09
37.35	7.47E-10	9.64E-10	8.17E-10	1.81E-09	1.53E-09	1.28E-09
37.75	1.12E-09	1.19E-09	1.10E-09	1.80E-09	1.62E-09	1.17E-09
38.15	9.67E-10	1.15E-09	1.17E-09	1.55E-09	1.27E-09	1.51E-09
38.55	8.44E-10	7.91E-10	8.77E-10	1.75E-09	1.52E-09	1.15E-09
38.96	9.17E-10	1.06E-09	8.87E-10	1.75E-09	1.37E-09	1.86E-09
39.36	8.70E-10	1.28E-09	1.17E-09	1.76E-09	1.34E-09	1.64E-09
39.76	1.35E-09	9.40E-10	8.48E-10	1.55E-09	1.47E-09	1.29E-09
40.16	1.11E-09	1.29E-09	9.29E-10	1.66E-09	1.68E-09	1.14E-09
40.56	7.53E-10	1.16E-09	9.76E-10	1.67E-09	1.72E-09	9.82E-10
40.96	1.36E-09	1.01E-09	1.05E-09	1.56E-09	1.23E-09	1.14E-09
41.36	1.49E-09	1.14E-09	9.80E-10	1.76E-09	1.67E-09	1.70E-09
41.77	9.38E-10	1.07E-09	8.10E-10	1.29E-09	1.40E-09	1.56E-09
42.17	1.23E-09	8.98E-10	9.39E-10	1.52E-09	1.35E-09	1.54E-09
42.57	1.03E-09	1.36E-09	9.20E-10	1.49E-09	1.06E-09	9.96E-10
42.97	8.38E-10	9.38E-10	9.04E-10	1.48E-09	1.52E-09	1.06E-09
43.37	8.14E-10	8.87E-10	1.00E-09	1.93E-09	1.22E-09	1.18E-09
43.77	7.93E-10	8.03E-10	8.75E-10	1.43E-09	1.11E-09	1.38E-09
44.18	1.06E-09	8.82E-10	9.44E-10	1.39E-09	1.15E-09	1.28E-09
44.58	1.36E-09	7.38E-10	1.01E-09	1.10E-09	1.06E-09	1.24E-09
44.98	1.34E-09	1.03E-09	9.54E-10	1.66E-09	1.27E-09	1.13E-09
45.38	9.98E-10	6.77E-10	1.10E-09	1.32E-09	8.71E-10	9.04E-10
45.78	1.17E-09	9.06E-10	1.07E-09	1.37E-09	1.10E-09	1.41E-09
46.18	1.10E-09	1.07E-09	6.90E-10	1.18E-09	9.14E-10	1.50E-09
46.59	1.24E-09	1.03E-09	1.08E-09	1.65E-09	1.03E-09	1.22E-09
46.99	1.06E-09	8.67E-10	1.27E-09	1.48E-09	1.16E-09	1.22E-09
47.39	1.29E-09	9.91E-10	9.56E-10	1.74E-09	9.90E-10	1.02E-09
47.79	9.21E-10	1.21E-09	8.66E-10	1.37E-09	1.43E-09	1.17E-09
48.19	1.11E-09	7.83E-10	9.25E-10	1.58E-09	1.35E-09	9.35E-10
48.59	1.39E-09	1.11E-09	8.84E-10	1.19E-09	1.24E-09	1.08E-09
49.00	1.08E-09	6.00E-10	1.47E-09	1.19E-09	1.12E-09	7.44E-10
49.40	1.65E-09	1.08E-09	1.38E-09	1.43E-09	1.05E-09	7.89E-10
49.80	1.45E-09	1.11E-09	9.40E-10	1.42E-09	1.51E-09	1.52E-09
50.20	9.59E-10	1.35E-09	8.69E-10	1.30E-09	1.02E-09	1.20E-09
50.60	7.99E-10	1.08E-09	7.26E-10	1.15E-09	1.28E-09	8.49E-10
51.00	1.08E-09	1.53E-09	1.16E-09	1.38E-09	1.60E-09	7.93E-10
51.40	9.11E-10	1.03E-09	1.56E-09	1.69E-09	1.38E-09	9.82E-10
51.81	1.22E-09	6.53E-10	1.00E-09	1.49E-09	1.15E-09	9.69E-10
52.21	1.09E-09	9.22E-10	1.02E-09	1.27E-09	1.26E-09	1.31E-09
52.61	9.37E-10	1.13E-09	1.14E-09	1.43E-09	1.16E-09	8.15E-10
53.01	7.61E-10	7.67E-10	1.13E-09	1.22E-09	9.33E-10	9.91E-10
53.41	1.15E-09	1.17E-09	1.30E-09	9.32E-10	9.39E-10	1.10E-09



53.81	1.02E-09	1.18E-09	1.11E-09	1.30E-09	1.20E-09	1.36E-09
54.22	1.20E-09	8.49E-10	1.16E-09	1.41E-09	1.20E-09	1.12E-09
54.62	1.11E-09	1.27E-09	1.00E-09	1.54E-09	9.35E-10	1.02E-09
55.02	1.04E-09	1.02E-09	1.23E-09	1.30E-09	7.95E-10	9.41E-10
55.42	1.05E-09	1.09E-09	1.01E-09	1.21E-09	1.06E-09	9.27E-10
55.82	1.12E-09	1.13E-09	9.42E-10	1.08E-09	1.22E-09	8.98E-10
56.22	1.25E-09	6.59E-10	1.12E-09	1.20E-09	1.05E-09	1.11E-09
56.63	1.12E-09	8.20E-10	1.26E-09	1.37E-09	9.39E-10	1.13E-09
57.03	8.86E-10	1.15E-09	1.24E-09	8.25E-10	9.48E-10	1.29E-09
57.43	1.32E-09	9.25E-10	1.13E-09	1.23E-09	1.10E-09	9.66E-10
57.83	1.03E-09	8.69E-10	8.49E-10	9.70E-10	1.12E-09	1.29E-09
58.23	1.32E-09	1.12E-09	6.14E-10	1.03E-09	9.94E-10	1.36E-09
58.63	1.04E-09	8.22E-10	9.58E-10	1.40E-09	8.87E-10	9.39E-10
59.04	9.66E-10	1.14E-09	9.08E-10	1.18E-09	8.89E-10	1.40E-09
59.44	1.05E-09	1.07E-09	1.06E-09	1.01E-09	1.06E-09	6.84E-10
59.84	1.15E-09	1.11E-09	1.09E-09	1.40E-09	1.21E-09	1.36E-09
60.24	1.42E-09	9.72E-10	7.76E-10	8.88E-10	1.02E-09	7.50E-10
60.64	1.26E-09	9.58E-10	1.01E-09	9.82E-10	1.30E-09	1.44E-09
61.04	8.79E-10	7.48E-10	8.38E-10	1.03E-09	8.56E-10	1.28E-09
61.44	1.30E-09	9.67E-10	1.17E-09	1.40E-09	1.27E-09	1.35E-09
61.85	1.21E-09	1.01E-09	7.26E-10	1.29E-09	1.33E-09	8.45E-10
62.25	1.25E-09	6.36E-10	8.57E-10	1.01E-09	1.08E-09	1.10E-09
62.65	1.28E-09	9.15E-10	1.18E-09	9.97E-10	7.16E-10	9.37E-10
63.05	1.04E-09	9.87E-10	1.03E-09	1.06E-09	1.06E-09	1.31E-09
63.45	1.16E-09	1.17E-09	9.90E-10	9.81E-10	9.25E-10	1.03E-09
63.85	1.33E-09	7.63E-10	9.61E-10	7.14E-10	1.10E-09	1.48E-09
64.26	1.32E-09	1.34E-09	9.97E-10	8.50E-10	8.96E-10	1.08E-09
64.66	1.27E-09	1.07E-09	8.37E-10	8.37E-10	1.14E-09	9.78E-10
65.06	9.58E-10	1.06E-09	9.02E-10	8.12E-10	9.53E-10	8.25E-10
65.46	9.45E-10	1.14E-09	1.24E-09	7.82E-10	1.18E-09	9.80E-10
65.86	9.56E-10	1.36E-09	1.09E-09	1.00E-09	7.51E-10	1.06E-09
66.26	9.01E-10	8.28E-10	1.22E-09	1.26E-09	1.21E-09	1.16E-09
66.67	9.84E-10	8.98E-10	1.04E-09	8.15E-10	9.05E-10	7.63E-10
67.07	9.76E-10	9.82E-10	1.09E-09	8.68E-10	9.03E-10	1.03E-09
67.47	1.22E-09	9.51E-10	1.34E-09	1.09E-09	1.05E-09	1.05E-09
67.87	1.52E-09	8.73E-10	8.87E-10	1.17E-09	9.73E-10	1.22E-09
68.27	1.07E-09	8.30E-10	7.38E-10	1.35E-09	1.08E-09	9.60E-10
68.67	1.10E-09	9.20E-10	7.98E-10	9.95E-10	1.29E-09	1.50E-09
69.08	1.57E-09	1.01E-09	1.28E-09	1.12E-09	1.06E-09	1.11E-09
69.48	1.23E-09	7.59E-10	1.27E-09	7.28E-10	7.30E-10	1.13E-09
69.88	1.19E-09	1.32E-09	7.74E-10	1.10E-09	9.43E-10	9.85E-10
70.28	1.73E-09	8.65E-10	1.18E-09	8.34E-10	1.14E-09	1.12E-09
70.68	1.31E-09	1.01E-09	6.71E-10	1.29E-09	9.49E-10	1.16E-09
71.08	1.14E-09	9.39E-10	1.13E-09	9.47E-10	7.66E-10	1.21E-09
71.48	8.08E-10	9.40E-10	1.14E-09	8.80E-10	9.67E-10	8.66E-10



71.89	1.04E-09	9.97E-10	1.13E-09	9.67E-10	1.22E-09	9.39E-10
72.29	8.78E-10	1.25E-09	9.90E-10	7.58E-10	9.02E-10	1.14E-09
72.69	1.24E-09	9.15E-10	9.15E-10	7.55E-10	7.89E-10	8.99E-10
73.09	7.93E-10	1.17E-09	9.63E-10	9.34E-10	1.11E-09	1.17E-09
73.49	1.09E-09	6.47E-10	1.03E-09	9.83E-10	1.12E-09	6.07E-10
73.89	1.25E-09	1.04E-09	9.00E-10	8.75E-10	6.44E-10	1.51E-09
74.30	1.23E-09	8.60E-10	1.11E-09	8.48E-10	7.52E-10	9.16E-10
74.70	1.17E-09	1.08E-09	1.18E-09	1.05E-09	1.05E-09	7.25E-10
75.10	9.60E-10	1.11E-09	1.06E-09	1.12E-09	9.55E-10	9.92E-10
75.50	1.10E-09	1.29E-09	1.07E-09	8.89E-10	9.19E-10	1.09E-09
75.90	1.71E-09	1.12E-09	1.12E-09	9.04E-10	8.58E-10	9.53E-10
76.30	9.92E-10	9.18E-10	8.85E-10	1.10E-09	9.36E-10	9.65E-10
76.71	1.02E-09	8.49E-10	9.35E-10	8.85E-10	1.04E-09	1.05E-09
77.11	1.22E-09	9.57E-10	7.61E-10	8.77E-10	7.90E-10	8.75E-10
77.51	1.24E-09	7.54E-10	8.30E-10	1.42E-09	8.19E-10	1.31E-09
77.91	1.26E-09	8.89E-10	8.50E-10	1.05E-09	1.17E-09	1.21E-09
78.31	1.18E-09	7.39E-10	7.31E-10	9.28E-10	6.19E-10	9.65E-10
78.71	1.02E-09	1.04E-09	1.12E-09	8.40E-10	7.42E-10	9.66E-10
79.12	1.28E-09	1.09E-09	8.35E-10	1.21E-09	8.60E-10	1.09E-09
79.52	1.54E-09	8.44E-10	7.49E-10	8.88E-10	9.58E-10	1.44E-09
79.92	1.07E-09	7.97E-10	1.00E-09	8.83E-10	7.62E-10	8.74E-10
80.32	1.02E-09	7.14E-10	9.50E-10	9.29E-10	7.35E-10	1.30E-09
80.72	1.16E-09	1.01E-09	1.14E-09	1.01E-09	7.07E-10	1.09E-09
81.12	1.21E-09	8.44E-10	1.03E-09	9.47E-10	9.29E-10	1.19E-09
81.52	1.56E-09	1.11E-09	6.96E-10	8.73E-10	9.22E-10	9.94E-10
81.93	9.83E-10	1.19E-09	8.65E-10	1.16E-09	9.93E-10	1.21E-09
82.33	1.30E-09	6.86E-10	8.95E-10	1.16E-09	9.09E-10	1.49E-09
82.73	1.19E-09	1.04E-09	9.17E-10	9.55E-10	9.65E-10	1.32E-09
83.13	1.30E-09	8.31E-10	1.22E-09	9.21E-10	9.44E-10	1.13E-09
83.53	1.30E-09	1.01E-09	1.13E-09	1.01E-09	9.10E-10	1.24E-09
83.93	1.00E-09	7.56E-10	8.65E-10	8.57E-10	1.28E-09	1.19E-09
84.34	9.97E-10	8.99E-10	9.07E-10	9.74E-10	9.83E-10	1.14E-09
84.74	1.29E-09	1.23E-09	1.16E-09	1.03E-09	8.82E-10	1.28E-09
85.14	1.06E-09	8.93E-10	1.16E-09	1.18E-09	9.75E-10	1.17E-09
85.54	8.42E-10	8.65E-10	1.19E-09	9.50E-10	9.33E-10	1.40E-09
85.94	1.29E-09	8.69E-10	1.30E-09	8.24E-10	9.26E-10	1.66E-09
86.34	1.15E-09	8.68E-10	1.22E-09	8.53E-10	1.20E-09	1.56E-09
86.75	9.50E-10	6.99E-10	8.73E-10	1.06E-09	1.05E-09	1.39E-09
87.15	1.12E-09	7.82E-10	9.48E-10	1.10E-09	1.03E-09	1.32E-09
87.55	1.35E-09	9.62E-10	7.60E-10	1.04E-09	1.03E-09	1.67E-09
87.95	1.14E-09	9.30E-10	1.24E-09	9.75E-10	1.09E-09	1.11E-09
88.35	1.01E-09	1.07E-09	8.97E-10	6.89E-10	8.07E-10	1.09E-09
88.75	9.76E-10	8.03E-10	1.00E-09	1.01E-09	7.48E-10	1.41E-09
89.16	7.65E-10	8.31E-10	9.18E-10	7.78E-10	9.91E-10	1.33E-09
89.56	1.09E-09	7.96E-10	8.18E-10	7.37E-10	1.07E-09	1.05E-09



89.96	7.55E-10	9.55E-10	7.32E-10	8.56E-10	1.20E-09	1.13E-09
90.36	1.29E-09	9.05E-10	8.47E-10	9.81E-10	1.01E-09	9.83E-10
90.76	9.24E-10	1.02E-09	9.53E-10	1.19E-09	7.39E-10	1.04E-09
91.16	1.06E-09	7.48E-10	1.12E-09	7.96E-10	7.98E-10	1.66E-09
91.56	1.05E-09	8.57E-10	1.01E-09	8.58E-10	9.77E-10	1.14E-09
91.97	1.47E-09	1.09E-09	9.46E-10	7.60E-10	6.27E-10	1.41E-09
92.37	9.38E-10	8.46E-10	9.63E-10	9.31E-10	1.09E-09	1.21E-09
92.77	9.63E-10	9.39E-10	8.88E-10	1.09E-09	1.16E-09	1.19E-09
93.17	1.21E-09	1.38E-09	9.17E-10	9.38E-10	1.37E-09	1.51E-09
93.57	1.69E-09	1.14E-09	1.10E-09	1.07E-09	1.08E-09	1.71E-09
93.97	1.53E-09	6.39E-10	1.50E-09	8.25E-10	1.09E-09	1.27E-09
94.38	9.38E-10	1.22E-09	1.71E-09	9.00E-10	8.91E-10	1.42E-09
94.78	1.17E-09	9.91E-10	9.33E-10	8.53E-10	8.28E-10	9.99E-10
95.18	1.12E-09	9.41E-10	1.44E-09	1.25E-09	7.90E-10	1.21E-09
95.58	1.61E-09	7.63E-10	9.61E-10	1.07E-09	6.79E-10	1.38E-09
95.98	1.21E-09	9.06E-10	7.86E-10	1.08E-09	9.16E-10	1.20E-09
96.38	1.02E-09	1.00E-09	9.38E-10	7.31E-10	7.96E-10	1.05E-09
96.79	8.94E-10	1.04E-09	8.26E-10	8.82E-10	1.10E-09	1.31E-09
97.19	1.58E-09	1.21E-09	8.00E-10	1.07E-09	7.70E-10	1.30E-09
97.59	1.02E-09	1.03E-09	6.72E-10	9.81E-10	1.15E-09	1.93E-09
97.99	1.16E-09	9.83E-10	7.46E-10	9.68E-10	8.74E-10	1.45E-09
98.39	9.28E-10	8.64E-10	1.15E-09	1.06E-09	8.20E-10	1.62E-09
98.79	1.08E-09	9.16E-10	7.23E-10	1.30E-09	1.12E-09	1.32E-09
99.20	1.41E-09	1.13E-09	1.13E-09	1.25E-09	1.21E-09	1.38E-09
99.60	9.45E-10	6.59E-10	1.15E-09	9.01E-10	9.49E-10	1.37E-09
100.00	1.73E-09	1.14E-09	1.00E-09	9.24E-10	9.80E-10	1.27E-09



**APPENDIX B**  
**DATA FOR EXPERIMENT 7**

Distance (cm)	Without toroid	With 4 toroids
0	9.43E-09	7.61E-09
2	1.05E-08	1.53E-08
5	1.12E-08	1.41E-08
7	1.33E-08	1.55E-08
10	1.29E-08	1.59E-08
12	1.86E-08	1.72E-08
15	1.74E-08	2.15E-08
17	2.45E-08	2.18E-08
20	2.31E-08	2.49E-08
22	3.30E-08	2.55E-08
25	3.67E-08	2.23E-08
27	4.51E-08	3.68E-08
30	5.42E-08	4.58E-08
32	5.92E-08	5.57E-08
35	7.37E-08	5.70E-08
37	7.64E-08	5.08E-08
39	9.38E-08	5.20E-08
42	9.40E-08	7.71E-08
44	1.14E-07	1.02E-07
47	1.11E-07	1.10E-07
49	1.34E-07	1.06E-07
52	1.23E-07	7.67E-08
54	1.51E-07	9.29E-08
57	1.25E-07	1.42E-07
59	1.65E-07	1.69E-07
62	1.52E-07	1.69E-07
64	1.76E-07	1.46E-07
67	1.71E-07	1.03E-07
69	1.83E-07	1.47E-07
72	1.87E-07	2.05E-07
74	1.90E-07	2.15E-07
76	1.93E-07	2.09E-07
79	1.92E-07	1.68E-07
81	1.94E-07	1.19E-07
84	1.90E-07	1.75E-07
86	1.93E-07	2.12E-07
89	1.78E-07	2.13E-07
91	1.91E-07	1.99E-07
94	1.59E-07	1.58E-07
96	1.85E-07	1.18E-07
99	1.57E-07	1.65E-07
101	1.77E-07	1.84E-07
104	1.60E-07	1.85E-07
106	1.67E-07	1.73E-07

108	1.55E-07	1.33E-07
111	1.55E-07	1.05E-07
113	1.43E-07	1.34E-07
116	1.43E-07	1.46E-07
118	1.32E-07	1.46E-07
121	1.26E-07	1.32E-07
123	1.21E-07	9.56E-08
126	1.09E-07	7.30E-08
128	1.10E-07	8.53E-08
131	9.15E-08	8.97E-08
133	9.76E-08	8.90E-08
136	7.58E-08	7.47E-08
138	8.25E-08	5.53E-08
141	6.26E-08	4.53E-08
143	6.44E-08	4.76E-08
145	4.50E-08	5.00E-08
148	4.45E-08	4.66E-08
150	2.78E-08	3.83E-08
153	2.70E-08	3.09E-08
155	1.26E-08	2.61E-08
158	1.22E-08	2.70E-08
160	9.82E-09	2.70E-08
163	1.46E-08	2.42E-08
165	1.51E-08	2.14E-08
168	1.88E-08	1.89E-08
170	1.82E-08	1.58E-08
173	1.99E-08	1.55E-08
175	1.98E-08	1.43E-08
178	1.99E-08	1.21E-08
180	2.00E-08	1.11E-08